

Ultra-luminous X-ray Sources in nearby galaxies from ROSAT HRI observations II. statistical properties

Ji-Feng Liu, Joel N. Bregman, and Jimmy Irwin

Astronomy Department, University of Michigan, MI 48109

ABSTRACT

The statistical properties of the ultra-luminous X-ray source (ULX) populations extracted from the ROSAT HRI survey of X-ray point sources in nearby galaxies in Paper I are studied to reveal connections between the ULX phenomenon and survey galaxy properties. The $\log N$ – $\log S$ relation is used to calculate and remove the influence of false ULXs from the background and/or foreground objects. Study of the luminosity functions shows that the regular ULXs below 10^{40} erg/sec are an extension of the ordinary HMXB/LMXB population below 10^{39} erg/sec in the late-type galaxies, and that the extreme ULXs above 10^{40} erg/sec might be a different population from the regular ULXs. This survey confirms statistically that the ULX phenomenon is closely connected to star formation activities, since ULXs preferentially occur in late-type galaxies rather than in early-type galaxies, and ULXs in late-type galaxies tend to trace the spiral arms. Only 5% of the early-type galaxies host ULXs above 10^{39} erg/sec, with 0.02 ± 0.10 ULX per survey galaxy and -0.13 ± 0.09 ULXs per $10^{10} L_{\odot}$ that are consistent with being zeros. In contrast, 45% of the late-type galaxies host at least one ULX, with 0.72 ± 0.11 ULXs per survey galaxy and 0.84 ± 0.13 ULXs per $10^{10} L_{\odot}$. 70% of the starburst galaxies host at least one ULX, with 0.98 ± 0.20 ULXs per survey galaxy and 1.5 ± 0.29 ULXs per $10^{10} L_{\odot}$. An increasing trend of the occurrence frequencies and ULX rates is revealed for galaxies with increasing star formation rates. Two ULX populations, the HMXB-like ULXs as an extension of the ordinary HMXB population associated with the young stellar population and the LMXB-like ULXs as an extension of the ordinary LMXB population associated with the old stellar population, are both required to account for the total ULX population. It is found that the LMXB-like ULXs dominate the ULX population at low star formation rates, while HMXB-like ULXs dominate at high star formation rates. However, an accurate quantitative description of the relative fractions of HMXB-like ULXs and LMXB-like ULXs is impossible

in the current HRI survey due to the source blending effects, and a Chandra survey of the X-ray point sources in nearby galaxies would be required for this purpose.

Subject headings: catalogs – galaxies: general – X-rays: binaries – X-rays: galaxies

1. INTRODUCTION

Ultra-luminous X-ray sources (ULXs) are extra-nuclear sources with luminosities in the range of $10^{39} - 10^{41}$ erg/sec in other galaxies, and have been observed by the Einstein Observatory (e.g., Fabbiano et al. 1989), ROSAT (e.g., Colbert & Mushotzky 1999), ASCA (e.g., Makishima et al. 2000), and recently by the Chandra and XMM-Newton X-ray Observatories in many galaxies (e.g., Kilgard et al. 2002; Swartz et al. 2004). As compared to the cases of the X-ray binaries in our Galaxy, which are powered by accretion onto neutron stars or stellar mass black holes and have luminosities of $10^{33} - 10^{39}$ erg/sec, the luminosities of ULXs require accreting black holes of masses $10^2 - 10^4 M_{\odot}$ if they emit at 0.1–0.01 of the Eddington luminosity, typical of Galactic X-ray binaries (Colbert & Mushotzky 1999). Such intermediate mass black holes, if they exist, bridge the gap between stellar mass black holes and supermassive black holes of $10^6 - 10^9 M_{\odot}$ in the center of galaxies. Alternatively, ULXs could be stellar mass black holes or neutron stars whose apparent super-Eddington luminosities are due to some special processes. One suggestion is that radiation pressure-dominated accretion disks with photon-bubble instabilities are able to emit truly super-Eddington luminosities (Begelman 2002). Another suggestion is that beaming effects can produce the observed luminosities of ULXs (King et al. 2001).

The leading goals in ULX studies are to determine the masses of the primary, to understand how and where they form, and to find out how they emit at such high luminosities. In the last few years observations of many ULXs in nearby galaxies have been made to address these questions, and important clues have been revealed on their spectra (e.g., Makishima et al, 2000; Miller et al. 2003), their preferential occurrence in galaxies with current star forming activities (e.g., Kilgard et al. 2002; Zezas et al. 2002; Gao et al. 2003), their short-term and long-term variabilities, periodic variations (e.g., Sugihara et al. 2001; Bauer et al. 2001; Liu et al. 2002), and quasi-periodic oscillations (e.g., Strohmayer & Mushotzky 2003; Soria et al. 2004; Soria & Motch 2004; Liu et al. 2004). Aside from in-depth studies of some well-known ULXs, the study of a complete sample of ULXs, with incompleteness carefully calculated, is necessary to study the defining properties of ULXs as a class, and to calculate the occurrence rates and luminosity functions that will place constraints on models on how

ULXs form and evolve.

With observations of individual ULXs in nearby galaxies accumulating, now it is becoming feasible to construct samples with statistically significant number of ULXs. So far there are only a few such studies. Colbert & Ptak (2002, hereafter CP2002) analyzed the HRI observations to search for ULXs in a sample of 9999 galaxies in the Third Reference Catalog of galaxies (RC3; de Vaucouleurs et al. 1991) with $cz < 5000$ km/sec. They found 87 ULXs in 54 galaxies, with 37 in early-type galaxies. Based on this catalog, Ptak & Colbert (2004) found that $\sim 12\%$ of galaxies contain at least one ULX with $L_X \geq 10^{39}$ erg/sec and $\sim 1\%$ of galaxies contain at least one ULX with $L_X \geq 10^{40}$ erg/sec in 2–10 keV. However, many ULXs in the CP2002 catalog are projected far from the host galaxies, and may be foreground stars or background AGN/QSOs instead (Irwin et al. 2004). Recently Swartz et al. (2004) analyzed the archive Chandra ACIS observations for 82 nearby galaxies, in which they found 154 extranuclear point sources with $L_X \geq 10^{39}$ erg/sec in 0.5–8 keV as ULX candidates. They estimate a ULX rate of 1.5 ± 0.55 ULXs per $10^{10} M_\odot$ for spirals, and 0.55 ± 0.10 ULXs per $10^{10} M_\odot$ for early type galaxies. Based on a rough comparison of the cumulative luminosity functions of the ULXs to the Chandra Deep Field results they conclude $\sim 14\%$ (44%) of the ULXs in spiral (early-type) galaxies may be background objects.

We have carried out a survey of ULXs in nearby galaxies with ROSAT HRI archival data (Liu & Bregman, 2005; hereafter Paper I), which takes advantage of the moderate spatial resolution of HRI (with on-axis FWHM of $< 5''$) and the large sky coverage ($\sim 2\%$) of the data archive. This survey encompasses 313 galaxies within 40 Mpc with isophotal diameters $> 1'$ observed by 467 HRI observations, with an average of 2.2 observations per galaxy. Uniform data reduction procedures were applied to all observations to detect point sources with a wavelet detection algorithm, for which simulations were run to understand its behaviors on HRI observations, including the false detection rates, the detection thresholds, and the correction factors to correct detected counts to true source counts based on the detection significance and the off-axis angles of detected sources. As a result, 106 extranuclear point sources with $L_X \geq 10^{39}$ erg/sec in 0.3–8 keV defined as ULX candidates are found in the D_{25} isophotes of 63 galaxies, with ten already identified as QSOs or stars. There are 110 ULX candidates found between $1-2 \times D_{25}$ of 64 galaxies, with 16 already identified as QSOs or stars.

To minimize the contamination from background and/or foreground objects, in Paper I we constructed a clean sample of 109 ULXs from the ULX candidates by selecting only those within the D_{25} isophotes or with apparent connections with the host galaxy, and excluding those identified as QSOs and stars. The clean sample forms a good basis for studies on ULX's environments and identifications, since the contamination is small due to exclusion of known

QSOs and stars. The trend that ULXs are preferentially found in spiral galaxies is clearly shown in the clean sample, with 49 out of 181 spiral galaxies in our survey host 89 ULXs, while 4 out of 93 early-type galaxies host 7 ULXs if we exclude the 8 ULXs in two peculiar lenticular galaxies NGC1316 and NGC5128. However, it is inappropriate to compute the occurrence frequency of ULXs in spiral (early-type) galaxies with this clean sample, because the selection criteria for ULXs in this sample are not uniform, and the contamination from background and foreground objects, though small, is uncertain.

In this paper, we compute the occurrence rates and the luminosity functions of ULXs in different types of galaxies with the contamination carefully calculated and subtracted. In Section 2 we present the methodology used in our analysis, including how ULX samples are constructed from the HRI survey, how the contamination is calculated, what aspects of the samples are studied, and how the ULX rates are normalized by the surveyed blue light. We compare in Section 3 the statistical properties of ULX samples in different types of galaxies, including early-type galaxies, late type galaxies, starburst and non-starburst galaxies, and galaxies with different star formation rates. We study the radial distribution of ULXs with respect to the isophotal ellipses of the galaxies in Section 4. The paper is concluded by discussions on our results in Section 5.

2. METHODOLOGY

Statistical analysis of large samples of ULXs is essential to study ULXs as a class. There have been a few such studies, e.g., CP2002, Kilgard et al. (2002), Ptak & Colbert (2004), and Swartz et al. (2004), most of which do not have a thorough analysis of the contamination from background and foreground objects. Here we present our method for analyzing the ULX samples from our ROSAT HRI survey, with particular care on the contamination problem.

2.1. Construction of ULX samples

The total HRI survey includes 313 galaxies of different types with different properties. In our study, we divide the 313 galaxies into groups to study the connection between ULXs and the properties of the galaxies. Galaxies are grouped based on the morphological types of the galaxies to reveal possible trends of ULXs along the Hubble sequence. To study the connection between the star formation activities and the ULX phenomenon, we group the galaxies based on whether they are starburst or HII galaxies, and also based on the star formation rate inferred from the FIR luminosity.

A complete ULX sample is extracted from a snapshot survey of galaxies, in which a galaxy is observed in *one* observation, by selecting *all* extranuclear X-ray point sources within (parts of) the galaxies with $L_X > 10^{39}$ erg/sec. Such a sample is an instantaneous sample, which is different from the collection of ULX candidates from all 313 survey galaxies listed in Table 3 of Paper I, because the latter is collected from *multiple* observations of galaxies. Such a sample is also different from the clean sample of ULXs defined in Paper I, because some extranuclear sources identified as background QSOs and foreground stars are excluded from the clean sample.

To make a snapshot survey of the galaxies, one observation needs to be selected for each galaxy. One way is to select the observation with the longest exposure for each galaxy, which we refer as the deep survey. Another way is to select a random observation from all available for each galaxy to form a random survey. In our analysis, we compute 20 random surveys, the average of which is calculated and referred as the average survey. The ULX samples drawn from the average survey and the deep survey are usually different, because the X-ray sources vary in luminosity between observations, and the deep survey has larger low luminosity coverage than the average survey.

The ULX candidates are grouped by their proximity to the galactic center into those within the D_{25} isophotes, and those between $1-2 \times D_{25}$. In our discussion, we focus on the statistical properties of the the ULX samples within the D_{25} isophotes of the galaxies, which presumably have a higher fraction of “true” ULXs than the ULX samples between $1-2 \times D_{25}$. To reveal how ULXs are distributed radially in galaxies, we study the ULX samples within annuli of the isophotes in Section 4, and compare the ULX sample between $1-2 \times D_{25}$ to the ULX sample within the D_{25} isophotes.

In the following sub-sections, we describe how we calculate the number of contaminating sources based on the $\log N-\log S$ relation, the survey blue light curve, the ULX rates, and luminosity functions for the ULX samples.

2.2. Contamination of ULX samples

ULXs are usually defined by associating an X-ray source to a galaxy based on its projected proximity to the galaxy. Such a definition inevitably introduces into a ULX sample the contamination from foreground and/or background objects, which must be excluded when studying the statistical properties of the ULX sample. A direct way is to make deep optical and/or spectroscopic observations of every ULX candidate in a sample, identify those foreground and/or background objects, and exclude them from the sample. However, it is

impractical to make such studies for all ULXs in a large sample considering the huge amount of telescope time needed, although optical and spectroscopic studies of a number of ULXs are essential and have to be made to determine the nature of the ULX systems.

A practical way to estimate the contamination from background and foreground objects, as used in this paper, is to make predictions with a logN–logS relation, and exclude the predicted numbers from the ULX sample in the statistical studies that follow. For the HRI observations in this survey, it is appropriate to use the logN–logS relation derived from ROSAT observations (Hasinger et al. 1998), where the differential form is $dN/dS = N_1 S^{-\beta_1}$ for $S > S_b$ and $dN/dS = N_2 S^{-\beta_2}$ for $S < S_b$, with S in unit of 10^{-14} erg/sec/cm², $S_b = 2.66 \pm 0.66$, $N_2 = 111 \pm 10$, $\beta_1 = 2.72 \pm 0.27$, $\beta_2 = 1.94 \pm 0.19$, and $N_1 = 238.1$. With this differential relation, the number of contaminating sources in a flux interval can be calculated with the survey area curve $A(>S)$ that gives the area (i.e., solid angle) in which sources brighter than the limiting flux S can be detected in the survey. A typical error of 10% is associated with the predicted number of contaminating sources.

The survey area curve $A(>S)$ can be calculated for an observation given the sensitivity (detection threshold) of the observation. For our data reduction procedures, the 3σ detection threshold can be computed with the background level and the source size that has been derived from simulations in Paper I as a function of the off-axis angle θ . A sensitivity map is constructed for each observation by computing the detection thresholds (in unit of count/sec) at the location of every pixel, with the average background level computed from the part of the detector with off-axis angle $\theta < 17'$ excluding the detected sources. The survey area curve $A(>S)$ for a galaxy in this observation can be computed by summing up the area of the pixels within this galaxy for which the detection thresholds correspond to flux less than S . Similarly, the survey area curves for parts of a galaxy, e.g., the region between $1-2 \times D_{25}$, can be computed by considering only pixels within those parts.

The detection threshold in count rate is converted to flux S by assuming a power law spectrum, using Galactic HI column density toward the galaxy, with a photon index of 2 within 0.5–2.4 keV to be consistent with what was used in the derivation of the logN–logS relation (Hasinger et al. 1998). Note that the flux S for use in the logN–logS relation is different from the apparent flux F , used to calculate the luminosity L in Paper I, because for the flux F we used a power-law spectrum with a photon index of 1.7 within 0.3–8.0 keV to be comparable to Chandra observations. The flux F is higher than S by a factor of ~ 3 for the same count rate, with the factor varying slightly with the Galactic HI column density used in the conversions.

Given the survey area curve $A(>S)$ for a galaxy in an observation, the number of background and foreground objects can be calculated by integrating the product of dN/dS

and $A(>S)$ over flux intervals. The number $N_b(S_1, S_2)$ over a flux interval of (S_1, S_2) is

$$N_b(S_1, S_2) = \int_{S_1}^{S_2} \frac{dN}{dS} A(>S) dS$$

To estimate the number $N_b(L_1, L_2)$ for a galaxy in an apparent luminosity bin (L_1, L_2) , the luminosity L is converted to S using a function $S_g(L)$ with the distance to the galaxy, and with proper consideration of the different conversion factors from the count rate to flux S and flux F . For a group of galaxies, the total number $N_b(L_1, L_2)$ can be calculated by summing up the numbers for individual galaxy in their respective observation, i.e.,

$$N_b(L_1, L_2) = \sum_g \int_{S_g(L_1)}^{S_g(L_2)} \frac{dN}{dS} A_g(>S) dS$$

Here $S_g(L)$ has a dependence on the distance of the galaxy and the Galactic HI column density toward the galaxy.

2.3. Blue light surveyed in ULX surveys

The occurrence rates of ULXs in different types of galaxies place constraints on models on how ULXs form and evolve. The occurrence rate can be directly calculated as the number of ULXs per galaxy, or calculated as the number of galaxies per unit stellar mass to account for the variations in the size and stellar mass of galaxies among and within different types. The stellar mass content of a galaxy can be inferred from the total light of the galaxy with the stellar mass-to-light ratio. While the mass-to-light ratios have larger variations in the optical than in the near-infrared (Bell & De Jong, 2001), in our analysis we use the blue light from RC3 and calculate the number of ULXs per $10^{10} L_\odot$ of blue light, due to the lack of a uniform compilation of near-infrared magnitudes for the survey galaxies.

The survey blue light curve $\mathcal{L}_g(L)$ for a galaxy gives the blue light of the stellar contents in which X-ray sources above L can be detected in an observation. To compute the detection threshold in L , we calculate the detection threshold in count rate for each pixel of the HRI image as described in Section 2.2, convert it to flux F by using a power-law spectrum with a photon index of 1.7 in 0.3–8 keV, and calculate $L = 4\pi D^2 F$ with D as the distance to the galaxy. To compute the blue light, we compute the light profile for the galaxy from the total blue light \mathcal{L}_B and the effective radius R_e that encloses 50% of the total light. For two thirds of the survey galaxies, the effective radii are taken from RC3, with an average R_e of $0.15 \times D_{25}$. For one third of the survey galaxies without R_e from RC3, we assume $R_e = 0.15 \times D_{25}$. The blue magnitudes of 297 survey galaxies are taken from the RC3 catalog, and converted to blue light \mathcal{L}_B in unit of L_\odot with $M_{B\odot} = 5.46$ mag.

The light profile for early-type galaxies is usually expressed in the De Vaucouleurs $R^{1/4}$ law, which reads $I(R) = I_e 10^{3.33-3.33(R/R_e)^{1/4}}$. Here I_e is the surface brightness at the effective radius R_e , and the total light can be expressed as $7.22\pi R_e^2 I_e$. With R_e and \mathcal{L}_B known, the light profile can be expressed as $I(R) = \frac{\mathcal{L}_B}{7.22\pi R_e^2} 10^{3.33-3.33(R/R_e)^{1/4}}$.

The light profile for late-type galaxies is decomposed into a De Vaucouleurs bulge in the form of $I(R) = I_e 10^{3.33-3.33(R/r_e)^{1/4}}$, and an exponential disk in the form of $I(R) = I_0 e^{-R/h}$, with h as the scale height, I_0 as the surface-brightness at the galactic center, and the total light from the disk as $2\pi h^2 I_0$. The relative prominence of the two components change with the Hubble type T , and the bulge-to-disk (B/D) ratios, taken from Graham (2001) and interpolated when necessary, change from 25% at $T=0$ to 1% at $T=10$ with a general decrease toward later galaxy types. In spite of the variation in bulge-to-disk ratios, the r_e/h ratio is found to be quite constant, and we take $r_e/h = 0.2$ following Graham (2001). By assuming the effective radius R_e derived from RC3 encloses 50% of the disk light, we find $h = R_e/1.7$, $r_e = R_e/8.5$. This assumption is reasonable for most of the survey galaxies for which $B/D \ll 1$; for galaxies with non-negligible bulges, this slightly overestimates r_e and h . Given \mathcal{L}_B from RC3, we find $I_0 = \frac{\mathcal{L}_B}{1+B/D} \frac{1.7^2}{2\pi R_e^2}$, and $I_e = \frac{\mathcal{L}_B}{D/B+1} \frac{8.5^2}{7.22\pi R_e^2}$. With r_e, h, I_e , and I_0 calculated from R_e and \mathcal{L}_B , the light profile can be calculated with $I(R) = I_e 10^{3.33-3.33(R/r_e)^{1/4}} + I_0 e^{-R/h}$.

The survey blue light curve $\mathcal{L}_g(L)$ for a galaxy can be computed by summing up the blue light in pixels within the galaxy for which the detection thresholds correspond to luminosities below L . Similarly, the curve $\mathcal{L}_g(L)$ for parts of a galaxy, e.g., the region between $1-2 \times D_{25}$, can be computed by considering only pixels within those parts. The survey light curves $\mathcal{L}_g(L)$ are computed for (parts of) the 297 survey galaxies in different observations with the same procedures. The total survey light curve $\mathcal{L}(L)$ for a group of galaxies is computed by summing up the survey light curves of individual galaxies in their respective observations.

2.4. Statistical descriptions of ULX samples

With the contamination and the survey blue light computed for a survey, we study the statistical properties of the ULX population extracted from this survey by calculating the fractions of survey galaxies that host ULXs, the ULX rates per galaxy, the ULX rates per unit stellar light, and the luminosity function. The calculations are carried out for ULXs above different luminosities to study the evolution with luminosity.

Some basic quantities are calculated for a survey of galaxies. For a luminosity bin (L_1, L_2) , we calculate the observed number of ULXs $U_g(L_1, L_2)$ in each galaxy and the

observed total number of ULXs $U(L_1, L_2)$ in all galaxies, the predicted number of contaminating sources $N_b^g(L_1, L_2)$ for each galaxy and the total number $N_b(L_1, L_2)$ for all galaxies, the survey blue light curve $\mathcal{L}_g(L)$ for each galaxy and the total survey blue light curve $\mathcal{L}(L)$ for all galaxies. The net number of ULXs for a survey in a luminosity bin (L_1, L_2) is calculated as $N_t(L_1, L_2) = U(L_1, L_2) - N_b(L_1, L_2)$, with the nominal 1σ error as the maximum of $\sqrt{U(L_1, L_2)}$ and unity. The corresponding cumulative quantities, the observed cumulative number of ULXs $U(>L_1)$, the cumulative number of contaminating sources $N_b(>L_1)$, the cumulative net number of ULXs $N_t(>L_1)$ and its error, are calculated with L_2 set to 10^{42} erg/sec.

The occurrence frequency, i.e., the fraction of survey galaxies that host ULXs with luminosities above L is calculated by comparing the number of survey galaxies for which ULXs with luminosities above L can be detected and the number that host ULXs with luminosities above L . The former, $N_{Sg>(>L)$, is defined as the number of galaxies for which at least 10% of the blue light \mathcal{L}_g have detection thresholds below L . The latter, $N_{Hg>(>L)$, is defined as the number of galaxies for which $U_g(>L) - N_b^g(>L) > 0.95$, i.e., a galaxy with one ULX candidate and <0.05 contaminating sources is considered as a host galaxy. With these two numbers, the occurrence frequency is calculated as the minimum of 100% and $N_{Hg>(>L)/N_{Sg>(>L)}$.

The ULX rates per survey/host galaxy are calculated for ULXs with luminosities above L . The ULX rate per survey galaxy is calculated as $N_t^S(>L)/N_{Sg>(>L)$ with $N_t^S(>L)$ as the net number of ULXs in these $N_{Sg>(>L)$ survey galaxies. The error for $N_t^S(>L)$ is the maximum of unity and $\sqrt{U^S(>L)}$ with $U^S(>L)$ as the observed number of ULXs in these survey galaxies. Similarly, the ULX rate per host galaxy is calculated as $N_t^H(>L)/N_{Hg>(>L)$ with $N_t^H(>L)$ as the net number of ULXs in the $N_{Hg>(>L)$ host galaxies. The error for $N_t^H(>L)$ is the maximum of unity and $\sqrt{U^H(>L)}$ with $U^H(>L)$ as the observed number of ULXs in these host galaxies.

The ULX rate is also calculated as the number of ULXs per unit blue stellar light to account for the variable sizes of survey galaxies. For a bin (L_1, L_2) , the rate is calculated as

$$R(L_1, L_2) = \sum_{L_1 \leq L_i \leq L_2} \frac{1}{\mathcal{L}(L_i)} - \int_{L_1}^{L_2} \frac{dN_b(L, L + dL)}{\mathcal{L}(L)}$$

Here the sum is over all observed ULXs in the bin, and gives the observed ULX rate; the integral gives the contamination rate, with $dN_b(L, L + dL)$ as the number of contaminating sources in the luminosity interval $(L, L + dL)$. The error $E(L_1, L_2)$ is computed as

$$E^2(L_1, L_2) = \sum_{L_1 \leq L_i \leq L_2} \frac{1}{\mathcal{L}^2(L_i)}$$

If there are no observed ULXs in the bin, the error is defined as $E(L_1, L_2) = 1/\bar{\mathcal{L}}(L_1, L_2)$ with $\bar{\mathcal{L}}(L_1, L_2) = \int_{L_1}^{L_2} \mathcal{L}(L) dlgL / \int_{L_1}^{L_2} dlgL$ as the average of $\mathcal{L}(L)$ in the lgL space. If the survey light curve is a constant of \mathcal{L} in the bin, the above degenerates to $R(L_1, L_2) = \frac{U(L_1, L_2) - N_b(L_1, L_2)}{\mathcal{L}}$ and $E(L_1, L_2) = \frac{\sqrt{U(L_1, L_2)}}{\mathcal{L}}$. For a bin (L_1, L_2) , the cumulative ULX rate $R(>L_1)$ and its error $E(>L_1)$ are computed using the above expressions with L_2 set to 10^{42} erg/sec.

The above quantities are calculated for $L = 10^{38}$ erg/sec to $L = 10^{41}$ erg/sec in steps of $\Delta lgL = 0.2$. The quantities for some luminosities are tabulated to illustrate how they evolve with luminosity. In Table 1 the occurrence frequencies and ULX rates per galaxy are listed for ULXs above $lgL > 39/39.2/39.6/40$ in different surveys in our study. For each luminosity, we list (1) the number of survey galaxies, (2) the number of host galaxies, (3) the fraction, (4) the net number of ULXs per host galaxy, and (5) the net number of ULXs per survey galaxy. The ULX rates per unit stellar light for different surveys are listed in Table 2 for bins $lgL = [39, 39.2]$ and $lgL = [39.2, 39.4]$, and in Table 3 for bins $lgL = [39.6, 39.8]$ and $lgL = [40, 40.2]$. For each bin, we list (1) the observed number and the observed cumulative number of ULXs, (2) the number and the cumulative number of contaminating sources, (3) the net number of ULXs and its error, (4) the cumulative net number of ULXs and its error, (5) the average blue light in the bin, (6) the ULX rate and its error, and (7) the cumulative ULX rate and its error.

The luminosity function of X-ray point sources is calculated as the ULX rate per unit stellar light as a function of luminosity, in the luminosity range from 10^{38} erg/sec to 10^{41} erg/sec. Such a luminosity range covers ULXs and the luminous end for high-mass X-ray binaries (HMXBs) and low-mass X-ray binaries (LMXBs) commonly seen in our Galaxy and nearby galaxies, and enables direct comparisons between ULXs and HMXB/LMXBs. The luminosity function is fitted to the form of $dn/dL = \alpha L^{-\beta}$, i.e., $dn/dlgL = \alpha L^{-\beta+1}$, by minimizing

$$\chi^2(\alpha, \beta) \equiv \sum_i \frac{(N_t(L_i, L_{i+1}) - N_f(L_i, L_{i+1}))^2}{\sigma_i^2}$$

where $N_t(L_i, L_{i+1})$ is the net number of sources in the bin (L_i, L_{i+1}) , $N_f(L_i, L_{i+1}) = \int_{L_i}^{L_{i+1}} \alpha L^{-\beta} \mathcal{L}(L) dL$ is the number of sources predicted by the power-law model, and σ_i is the error as the maximum of unity and $\sqrt{U(L_i, L_{i+1})}$. The best fits are computed for ULX populations in some groups of galaxies. For each fit, the luminosity interval for the fit, α , β with their 68.3% errors, and the reduced χ^2 are listed in Table 4.

3. PROPERTIES OF DIFFERENT ULX SAMPLES

With the methods described in Section 2, here we discuss the statistical properties for the ULX sample from all survey galaxies, and samples from different groups of galaxies to reveal possible connections between the ULX phenomenon and the galaxy properties.

3.1. ULXs in all galaxies

The total HRI survey includes 313 galaxies, about 7.1% of the RC3 galaxies within 40 Mpc. Compared to the RC3 galaxies, the survey galaxies are slightly larger, closer, optically or X-ray brighter. In spite of slight over-abundances of ellipticals, lenticulars and S0/a–Sc early spirals, and an under-abundance of dwarf spirals and irregulars, the survey galaxy sample is representative of the nearby galaxies by morphological types. The ULX sample extracted from these galaxies is thus expected to be representative of surveys without large biases in galaxy types, and its properties can be used as standards to compare to properties of ULX samples from different groups of galaxies.

A deep survey is constructed from observations of all galaxies with the contamination from background/foreground objects carefully calculated following the procedures in Section 2. This surveys a total sky of 1.65 squared degrees and a total blue light of $2.3 \times 10^{12} L_{\odot}$, with an average sensitivity of about 2×10^{-14} erg/sec/cm² in flux and 4×10^{39} erg/sec in luminosity. With the $\log N$ – $\log S$ relation, 26 contaminating sources with apparent luminosities above 10^{39} erg/sec are predicted for the surveyed area within the isophotes of galaxies, about 29% of the 89 detected ULXs. The contamination rate is 30% (20.3/67) for ULXs above 1.6×10^{39} erg/sec, 26% (9/26) for ULXs above 4.0×10^{39} erg/sec, and 29% (2.6/9) for ULXs above 10^{40} erg/sec.

The occurrence frequencies and ULX rates are calculated with the procedures in section 2.4 and tabulated in Table 1–3. In the deep survey, there are 98 galaxies that could have a ULX above 10^{39} erg/sec detectable, and 35 galaxies (i.e., 36% of the 98 galaxies) host a net number of > 0.95 ULXs. This fraction is 25% (33/131) for ULXs above 1.6×10^{39} erg/sec, 8.8% (20/226) for ULXs above 4.0×10^{39} erg/sec, and 3% (8/281) for ULXs above 10^{40} erg/sec. The number of ULXs per survey galaxy is $0.56 \pm 0.08/0.32 \pm 0.06/0.10 \pm 0.02/0.02 \pm 0.01$ for ULXs above 1/1.6/4/ 10×10^{39} erg/sec. The ULX rate per $10^{10} L_{\odot}$ is $0.59 \pm 0.10/0.33 \pm 0.06/0.13 \pm 0.03/0.03 \pm 0.01$ for ULXs above 1/1.6/4/ 10×10^{39} erg/sec. Given the average of $\sim 0.8 \times 10^{10} L_{\odot}$ per survey galaxy, the ULX rates per $10^{10} M_{\odot}$ are consistent with the ULX rates per survey galaxy.

The occurrence frequencies can be compared to those given by Ptak & Colbert (2004).

In their HRI survey for ULXs in nearby galaxies, they compute the luminosities in 2–10 keV using a power-law spectrum with a photon index of 1.7, and the resultant luminosities are about 1.5 times lower than the luminosities computed in 0.3–8 keV in this survey. Ptak & Colbert (2004) find that the fraction of the survey galaxies that host more than one ULX is 12.3% for ULXs above 10^{39} erg/sec, 7.3% for ULXs above 2×10^{39} erg/sec, 3.1% for ULXs above 5×10^{39} erg/sec, and 1.1% for ULXs above 10^{40} erg/sec. These fractions are up to two times lower than the fractions computed from this survey after proper considerations of the difference in the luminosities. Note, however, that their criteria on whether a galaxy host a ULX are different from ours and tend to underestimate the number of host galaxies. For example, a galaxy is said to host ULXs in this survey if there are one detected ULX and 0.04 predicted contaminating sources, while it is not by their criteria.

An average survey is also computed for all galaxies in comparison to the deep survey. In the average survey, the occurrence frequency is 40% (34/84) for ULXs above 10^{39} erg/sec, 28% (32/113) for ULXs above 1.6×10^{39} erg/sec, 8.9% (19/212) for ULXs above 4×10^{39} erg/sec, and 3.8% (10/271) for ULXs above 10^{40} erg/sec. The ULX rate is $0.52 \pm 0.09/0.32 \pm 0.08/0.09 \pm 0.02/0.03 \pm 0.01$ ULXs per survey galaxy, and $0.70 \pm 0.12/0.38 \pm 0.07/0.11 \pm 0.03/0.04 \pm 0.02$ ULXs per $10^{10} L_{\odot}$ for ULXs above 1/1.6/4/ 10×10^{39} erg/sec. These occurrence frequencies and ULX rates are consistent with those in the deep survey; we will not list them for the surveys of galaxies in the following subsections.

The luminosity function of the X-ray point source populations, scaled by the surveyed blue light, is calculated in the luminosity range of 10^{38} – 10^{41} erg/sec (Figure 1). It can be well fitted with a power-law form $dn/dL = 0.56_{-0.19}^{+0.19} L^{-1.96_{-0.29}^{+0.40}}$ per $10^{10} L_{\odot}$ in the luminosity range of $2.5 \times 10^{38} - 10^{40}$ erg/sec (Table 4). At luminosities below 2×10^{38} erg/sec, the luminosity function drops from the power-law fit due to incompleteness. Despite the artificial classification of X-ray sources into HMXB/LMXBs and ULXs, there are no breaks, i.e., no changes of the slope or the normalization in the luminosity function around 10^{39} erg/sec between HMXB/LMXBs and ULXs. If the ULXs and HMXB/LMXBs are drawn from different binary distributions with different primary masses, binary properties and accretion rates, breaks in the combined luminosity function should be expected. The absence of such breaks, therefore, implies ULXs below 10^{40} erg/sec and the HMXB/LMXBs are drawn from the same binary distribution in spite of their different luminosity ranges.

A break in the luminosity function is present around 10^{40} erg/sec with marginal significance, which separates the regular ULXs below 10^{40} erg/sec and the extreme ULXs above 10^{40} erg/sec. For the bin at 10^{40} erg/sec, only one ULX is detected while the power-law fit would predict 5.0 true ULXs, and the $\log N$ – $\log S$ relation would predict 1.4 contaminating sources. The deficit of ULXs in this bin is on a 2.4σ significance level, if the number of

ULXs in this bin has a 1σ fluctuation of $\sqrt{5}$. As compared to the luminosity function for HMXB/LMXBs and the regular ULXs that decreases with the luminosity, the luminosity function flattens after the gap, though the ULX rates for the extreme ULX population are consistent with the power-law fit within the 1σ errors except for in the gap. For luminosities above 10^{40} erg/sec, nine extreme ULXs are detected, 2.6 contaminating sources are predicted, and 15.0 sources are expected from the power-law fit. The deficit of extreme ULXs is on a 2.2σ significance level, if the number of extreme ULXs has a 1σ fluctuation of $\sqrt{15}$. Such a break around 10^{40} erg/sec is expected as to separate the stellar mass X-ray binaries and intermediate mass X-ray binaries (Grimm et al. 2003). However, the significance for this break is marginal, and larger surveys with more ULXs would be required to test whether it is a true feature.

3.2. ULXs in galaxies of different types

In our analysis, the galaxies are divided into early-type galaxies, late-type galaxies and peculiar galaxies, and further into sub-types as elliptical, lenticular, Sa, Sb, Sc, Sd, and Sm galaxies based on the Hubble type T (Table 5). The survey galaxies cover a complete range of morphological types, and provide a chance to study the ULX populations in different types of galaxies with a uniform data set.

The contamination fraction of the ULX sample from the early-type galaxies is much higher than that from the late-type galaxies (Tables 2–3). In the deep survey of the early-type galaxies, 10 ULXs above 10^{39} erg/sec are detected, while 10.3 contaminating sources are predicted for its surveyed area of 0.33 squared degrees. For the late-type galaxies, 79 ULXs above 10^{39} erg/sec are detected, while 15.7 contaminating sources are predicted for its surveyed area of 1.32 squared degrees. The contamination fractions indicate that 63 (80%) of the ULXs from the late-type galaxies are true ULXs, and the ULX sample from the early-type galaxies is dominated by contaminating sources.

A significant preference for ULXs to occur in the late-type galaxies is clearly shown in the statistical results of the occurrence frequencies and ULX rates (Tables 1–3). The occurrence frequency for ULXs above 10^{39} erg/sec is 45% (34/76) in the late-type galaxies, 10 times higher than the 4.5% (1/22) in the early-type galaxies. For ULXs above $1.6/4/10 \times 10^{39}$ erg/sec, the occurrence frequencies are 31.2%/10.7%/3.1% in the late-type galaxies, much higher than the fractions of 8.6%/4.5%/2.3% in the early-type galaxies, though to lesser degrees for ULXs with higher luminosities. The ULX rates in the late-type galaxies are significantly higher than those in the early-type galaxies for the regular ULXs. For ULXs above 10^{39} erg/sec, for example, the ULX rate per survey galaxy in the late-type galaxies

(0.72 ± 0.11) is at least 5 times higher than that in the early-type galaxies (0.02 ± 0.11). For the extreme ULXs above 10^{40} erg/sec, the ULX rates in the late-type galaxies are still higher than those in the early-type galaxies, but they are consistent with each other within errors. Note that the ULX rates in the early-type galaxies are consistent with being zero, which reflects the equity between the number of detected ULXs and the number of contaminating sources.

The X-ray sources in the early-type galaxies are dominated by the LMXB population as seen from the luminosity function (Figure 2). Due to the lack of young massive stars in the early-type galaxies, most of the X-ray binary sources are LMXBs. In the deep (average) survey, the LMXB population shows a sharp cut-off at 10^{39} (1.6×10^{39}) erg/sec, which presumably corresponds to the Eddington luminosity of a $\sim 10M_{\odot}$ black hole. The rates of LMXBs in the early-type galaxies are much higher than those in the late-type galaxies and those from the power-law fit to the total X-ray population in all galaxies. In comparison, the ULX rates are low and consistent with being zero within 1σ errors for most luminosity bins; this reflects the equity between the number of detected ULXs and the number of contaminating sources. No power-law is fitted to the luminosity function of the ULX population separately due to the small number of detected ULXs in the early-type galaxies.

For the late-type galaxies, the luminosity function can be fitted with a power-law form of $dn/dL = 0.62_{-0.21}^{+0.21} L^{-1.73_{-0.25}^{+0.36}}$ per $10^{10} L_{\odot}$ in the luminosity range of $2.5 \times 10^{38} - 10^{40}$ erg/sec (Figure 3). This fit has a shallower slope than the power-law fit to the total X-ray population in all early-type and late-type galaxies, because the late-type galaxies have a significant ULX population while there is no significant ULX population in the early-type galaxies. Unlike in the early-type galaxies, there are no breaks in the luminosity function between the HMXB/LMXBs and the regular ULXs, indicating that the regular ULXs and the HMXB/LMXBs may be drawn from the same binary population in the late-type galaxies. Similar to the luminosity function from all galaxies, there is marginal evidence that the regular ULX population is different from the extreme ULX population, because of the flattening of the luminosity function for extreme ULXs, the deficit of extreme ULXs (significant on a 3.2σ level), and the gap (significant on a 2.4σ level) separating the two ULX populations.

The statistical properties of ULX samples from different sub-types of galaxies are calculated (Tables 1–3) to reveal possible trends with galaxy sub-types. The occurrence frequencies and ULX rates generally increase with the Hubble type T until they peak at Sc, then decrease with T (Figures 4–5). For Sc galaxies, the occurrence frequency (the ULX rate per survey galaxy) is 59% (1.10 ± 0.21) for ULXs above 10^{39} erg/sec, much higher than those for the average late-type galaxies and the early-type galaxies. When scaled by the survey blue

light, the ULX rates increases monotonically with T, and the rates in Sm spirals are highest among the sub-types of galaxies due to the small sizes of Sm spirals ($0.077 \times 10^{10} L_{\odot}$ per Sm galaxy as compared to $0.94 \times 10^{10} L_{\odot}$ per Sc galaxy).

The results of this HRI survey can be compared to the results of the recent Chandra ACIS survey of ULXs in 82 nearby galaxies (Swartz et al. 2004). For the Chandra survey, there are ~ 2 ULX candidates per galaxy for both early-type galaxies and late-type galaxies. The number of ULXs per unit (10^{42} erg/sec) blue luminosity is 0.11 ± 0.02 (0.30 ± 0.11) for early-type (late-type) galaxies, or 0.55 ± 0.10 (1.50 ± 0.55) ULXs per $10^{10} L_{\odot}$ given $L_{B\odot} \sim 5 \times 10^{32}$ erg/sec. These rates are higher than the rates from the HRI survey, especially for early-type galaxies. One reason for the rate difference lies in the different sensitivity ranges for HRI observations (0.5–2.4 keV) and ACIS observations (0.3–10 keV), which enables ACIS observations to detect highly absorbed ULXs buried in dust spiral arms. This is important given that $\geq 75\%$ of the ULXs (Paper I) are associated with spiral arms or other dust features. Another possible reason is the source blending effect, which is easier to occur in HRI observations for the poorer spatial resolution ($\sim 5''$) than in ACIS observations ($\sim 1''$). When the surface source density exceeds what the telescope can resolve, sources blend to reduce the number of sources and increase the diffuse X-ray background. A higher diffuse background increases the detection threshold, and lowers the luminosities of detected sources, both of which further reduce the number of detected sources.

3.3. ULXs in starburst and non-starburst galaxies

Many ULXs have been found to reside in star forming regions, which leads to the postulation that ULXs are closely related to star formation activities. The statistically significant preference for ULXs to occur in late-type galaxies as reported in the previous subsection is consistent with this postulation, since late-type galaxies are known to have star formation activities while few early-type galaxies have such activities. To study the connection between star formation and the ULX phenomenon, we group galaxies based on whether they are starburst galaxies that have significant *current* star formation activities. While no single definition of the starburst phenomenon exists, the survey galaxies listed as starburst or HII galaxies in NED are included in the starburst galaxy group (Sbrst), which include 46 out of 313 survey galaxies, with two E0 ellipticals, three dwarf lenticulars and 41 late-type galaxies. For comparison also constructed is another group of 164 non-starburst late-type galaxies (nSbrstL) that have milder star formation activities. We caution that the list of starburst/HII galaxies is not complete, and some galaxies in the non-starburst galaxy group may be starburst galaxies.

The contamination fraction of the ULX sample from the starburst galaxies is much lower than the fractions from non-starburst galaxies. In the deep survey of the starburst galaxies, 3.1 contaminating sources are predicted, while 35 ULXs above 10^{39} erg/sec are detected. The contamination fraction (9%) is much lower than that for non-starburst late-type galaxies (29%), and that for early-type galaxies (100%). The lowest contamination fraction implies that the starburst galaxies have the highest ULX surface density as compared to the other groups of galaxies, given that the number of contaminating sources is determined by the surface areas of the galaxies.

The occurrence frequencies and ULX rates in the starburst galaxies are higher than those in other types of galaxies. For ULXs above 10^{39} erg/sec, the occurrence frequency in starburst galaxies is 69% (18/26), much higher than that in the non-starburst late-type galaxies (31%) and that in the early-type galaxies (4.5%). The ULX rates per survey galaxy (per $10^{10}L_{\odot}$) in the starburst galaxies are 0.98 ± 0.20 (1.5 ± 0.29), about two times higher than those in the non-starburst late-type galaxies ($0.56 \pm 0.12/0.57 \pm 0.13$). For the extreme ULXs above 10^{40} erg/sec, the occurrence frequencies and ULX rates in the starburst galaxies are still higher than those in other types of galaxies, though to a lesser degree, and they are consistent with being the same within 1σ errors.

The difference of the ULX rates in starburst galaxies and non-starburst late-type galaxies can be used to estimate the ULX fractions due to *current* star formation. For ULXs above 10^{39} erg/sec, the difference is 0.93 ± 0.42 ULXs per $10^{10}L_{\odot}$, about 1.5 times of the ULX rate in the non-starburst late-type galaxies. This difference implies that about 60% of the ULXs in the starburst galaxies are linked to current star formation, if the difference is attributable exclusively to the current star formation. Note that this fraction is a lower limit since some of the “non-starburst” galaxies have high star formation rates as noted in the Section 3.4, and some of the ULXs may be linked to the star formation activities in these galaxies. For the extreme ULXs above 10^{40} erg/sec, the ULX rates in the starburst galaxies are higher than the rates in the non-starburst galaxies, however, only by an amount that is consistent with being zero within errors.

The luminosity function for the X-ray source population in the starburst galaxies (Figure 6) can be fitted with a power-law form of $dn/dL = 1.08_{-0.47}^{+0.47}L^{-1.73_{-0.35}^{+0.68}}$ per $10^{10}L_{\odot}$ in the luminosity range of $4 \times 10^{38} - 10^{40}$ erg/sec. There is no significant break between the HMXB/LMXB population and the regular ULX population, except for an insignificant deficit of sources in the luminosity bin of $6.3-10 \times 10^{38}$ erg/sec. The luminosity bin of $1.6-2.5 \times 10^{39}$ erg/sec is significantly lower than the best fit in the deep survey, yet may be a fluctuation in the counts, since the bin is consistent with the fit in the average survey. Similar to the luminosity function from the late-type galaxies, there is marginal evidence that the regular

ULX population is different from the extreme ULX population, because of the flattening of the luminosity function for extreme ULXs, the deficit of extreme ULXs (significant on a 1.5σ level), and the gap (significant on a 1.6σ level) separating the two ULX populations. This luminosity function is consistent with the universal luminosity function derived from Chandra observations of nearby starburst galaxies (Grimm et al. 2003), in that both show a similar power-law slope (~ 1.6), a cutoff around 10^{40} erg/sec, and no breaks around 10^{39} erg/sec.

The above power-law fit has a shallower slope and a normalization factor 2 times higher as compared to the power-law fit for the X-ray source population in the non-starburst late-type galaxies (Figure 7). The higher normalization indicates that the starburst galaxies have higher ULX rates than the non-starburst galaxies. The shallower slope indicates that the starburst galaxies have relatively more high luminosity ULXs than the non-starburst galaxies. However, this implication is not conclusive since the two slopes are consistent within the large fitting errors.

3.4. ULXs in galaxies with different star formation rates

As discovered in comparing ULXs in starburst and non-starburst galaxies, there are about two times more ULXs per $10^{10}L_{\odot}$ in starburst galaxies than in non-starburst galaxies. To quantify the relation between star formation and the ULX phenomenon, we group the galaxies based on their star formation rates. The star formation rate is calculated with $\text{SFR}(M_{\odot}/\text{yr}) = 4.5 \times 10^{-44} \times L(60\mu)$ (Rosa-Gonzalez et al. 2001). The flux densities at 60μ , listed in Table 1 of Paper I (Liu & Bregman 2005), are taken from the IRAS point source catalog (IPAC, 1986), with some nearby galaxies from Rice et al. (1988). For 102 galaxies that are not detected, the 3σ upper limit is calculated by adopting noise levels of 8.5 mJy/arcmin² (Rice et al. 1988). The calculated rates are compared to the compilation of Grimm et al. (2003) for 11 galaxies, and are consistent with their rates within 50% without systematic biases. Based on the calculated star formation rates, the galaxies are put into nine groups, each with similar star formation rates (Table 5).

The occurrence frequencies and ULX rates increase with the star formation rates of the galaxies (Tables 1–3). The occurrence frequency increases monotonically from $\sim 10\%$ for the group SFRU ($< 0.009M_{\odot}/\text{yr}$) to 80% for the group SFRD ($\sim 8.3M_{\odot}/\text{yr}$) for ULXs above 10^{39} erg/sec (Figure 8). The general increase trend of ULX rates shows large scatters for low luminosity ULXs, with a sharp drop from 1.5 ULXs above 10^{39} erg/sec per survey galaxy for the group SFRC ($\sim 2.1M_{\odot}/\text{yr}$) to 0.6 ULXs per survey galaxy for the group SFRD (Figure 9). This sharp drop is mainly attributable to the source blending effects, which would occur

and lead to fewer detected sources when the surface number density exceeds what the X-ray telescope can resolve. Comparison with Chandra observations shows that the blending effects reduce the detected ULXs significantly in HRI observations for the galaxies in the group SFRD. For the 15 galaxies with both HRI and ACIS observations, there are only 7 ULXs detected within the D_{25} isophotes in the HRI survey, while there are ~ 70 ULXs detected in ACIS observations. This number, 70 ULXs, exceeds the total numbers in the groups SFRC/H with similar total star formation rates, implying that these two groups are also affected by the blending effects, though to less degrees.

The general increase of ULX rates with the star formation rates tempts the postulation of a linear relation between the two quantities. Grimm et al. (2003) tested the postulation with Chandra observations of 11 nearby starburst galaxies with $\text{SFR} \geq 1M_{\odot}/\text{yr}$ in which the HMXBs dominate the X-ray sources, and found a universal luminosity function, i.e., $\frac{dN}{dL_{38}} = 3.3_{-0.8}^{+1.1} \text{SFR} L_{38}^{-1.61 \pm 0.12}$ for $L_c < 2 \times 10^{40}$ erg/sec, where L_{38} is the X-ray luminosity in units of 10^{38} erg/sec, and SFR is in units of M_{\odot}/yr . There are no breaks in the universal luminosity function between HMXBs and ULXs below L_c , indicating that the regular ULXs below L_c are an extension of the HMXB population in these starburst galaxies. The number of such HMXB-like ULXs expected from a galaxy is thus linearly proportional to the star formation rate of the host galaxy, i.e., $N_{ULX} = \beta \cdot \text{SFR}$. Here $\beta \sim 1.8/0.4/0.1$ for ULXs above $1/4/10 \times 10^{39}$ erg/sec. Note that the luminosity is calculated in 2–10 keV in Grimm et al. (2003), and is about 1.5 times lower than the luminosity in 0.3–8 KeV for a power-law spectrum with $\Gamma = 1.7$.

The expected linear relation between the number of ULXs and the star formation rate can be tested with the HRI survey. The star formation rates of the survey galaxies span from $< 0.001M_{\odot}/\text{yr}$ to $15M_{\odot}/\text{yr}$ with a median of $0.1 M_{\odot}/\text{yr}$, and many ($> 70\%$) galaxies are expected to host less than one ULX. To reduce the statistical fluctuation caused by the small number of ULXs in individual galaxies, we sum up the number of ULXs with the predicted contaminating sources subtracted and the star formation rate of each galaxy in a group. The linearity of the relation guarantees the same linear relation between the total number of ULXs and the total star formation rate for a group of galaxies. Here the total star formation rate (Tables 2–3) is calculated by summing up the star formation rates of only galaxies that can have ULXs detected. The expected linear relation is compared to the observed relation between the total number of ULXs and the total star formation rate calculated for the HRI survey (Figure 10). *The observed relations for ULXs above $1/4/10 \times 10^{39}$ erg/sec cannot be fitted with the expected linear relations, indicating that the ULXs are not a mere extension of the HMXB population.*

A tight non-linear correlation is shown between the total number of ULXs above 10^{39}

erg/sec ($N(L > 10^{39})$) and the total star formation rate. This can be fitted with $N(L_X > 10^{39}) = 7.0_{-1.9}^{+1.9} \text{SFR}^{0.36 \pm 0.07}$; the group SFRD is excluded from the fit for severe blending effects. For the galaxies with high star formation rates ($\geq 1 M_\odot/\text{yr}$, in groups SFRC/D/G/H), there are fewer ULXs detected than expected HMXB-like ULXs as an extension of the HMXB population, which may be attributed to the blending effects in these galaxies. For the galaxies with low star formation rates ($< 0.4 M_\odot/\text{yr}$, in groups SFRU/A/B/E/F), the expected HMXB-like ULXs are significantly fewer than the detected ULXs. These extra ULXs are an extension of the LMXB population in these galaxies given the dominance of LMXBs and the absence of breaks in the luminosity function between the LMXB and ULX populations. The HMXB-like ULXs correspond to the young X-ray point source population associated with the young stellar population (Pop I) as in Colbert et al. (2004), and the LMXB-like ULXs correspond to the old X-ray point source population associated with the old stellar population (Pop II).

The relative fractions of LMXB-like ULXs and HMXB-like ULXs change with the star formation rates of the galaxies. If the number of LMXB-like ULXs is linearly proportional to the total light and the the number of HMXB-like ULXs to the total star formation rate, the total number of ULXs can be expressed as $N = \alpha \cdot \mathcal{L} + \beta \cdot \text{SFR}$. Given the surveyed light and star formation rates, and the detected ULXs with the contaminating sources removed for groups SFRA and SFRC (Table 2), we get $\alpha = 0.93$ and $\beta = 0.20$ for ULXs above 10^{39} erg/sec. This relation underestimates the number of HMXB-like ULXs than predicted from the linear relation of Grimm et al (2003) due to the difference between HRI and ACIS in the sensitivity ranges, and the source blending effects at high star formation rates. For example, this relation predicts the group SFRD should have 15 ULXs, while there are ≥ 70 ULXs detected with Chandra observations. Nevertheless, this relation predicts correctly the trend that the LMXB-like ULXs dominate for low specific star formation rate ($\ll 4.6 M_\odot/\text{yr}/10^{10} L_\odot$), and the HMXB-like ULXs dominate for high specific star formation rate ($\gg 4.6 M_\odot/\text{yr}/10^{10} L_\odot$).

The total number of ULXs above 4×10^{39} erg/sec can be fitted with $N(L_X > 4 \times 10^{39}) = 3.5_{-1.7}^{+1.7} \text{SFR}^{0.13 \pm 0.13}$. This has a shallower slope than the fit for ULXs above 10^{39} erg/sec, and implies a steeper slope for the luminosity function of ULXs in galaxies with higher star formation rates. There is a seeming anti-example for this expectation, i.e., the luminosity function for ULXs in the starburst galaxies has a shallower slope than that in the non-starburst galaxies. This anti-example can be understood given the fact that, the starburst galaxies, while characterized by significant current star formation activities, have lower star formation rates than the non-starburst galaxies. About 60% (26/46) of the starburst/HII galaxies have rather low star formation rates ranging from 0.002 to $1 M_\odot/\text{yr}$ with a median of $0.06 M_\odot/\text{yr}$. In comparison, the non-starburst galaxies includes most of the galaxies with

highest star formation rates, including the two galaxies with the highest rates, four of the six galaxies with $> 10M_{\odot}/yr$, 14 of the 20 galaxies with $> 4M_{\odot}/yr$, and 27 of the 40 galaxies with $> 2M_{\odot}/yr$.

4. SPATIAL DISTRIBUTION OF ULXS

To study the spatial distribution of ULXs and how ULXs trace the blue light, we compare the ULX populations in elliptical annuli of the survey galaxies. For each galaxy, the area within $2 \times D_{25}$ is divided into twenty elliptical annuli in steps of $0.1 \times R_{25}$, with R_{25} as the elliptical radius of the D_{25} isophote. For a group of galaxies, we construct twenty ULX populations, with each extracted from the annuli of the same elliptical radius range. For each ULX population, the contamination and the survey blue light curve are calculated excluding the $10''$ nuclear region as described in Section 2. Here we study the radial distributions for ULXs in late-type galaxies and early-type galaxies.

There is a significant concentration of ULXs toward galactic centers in the late-type galaxies. The surface number density of ULXs above 10^{39} erg/sec, with the predicted contaminating sources subtracted, decreases with radii until it flattens outside the D_{25} isophotes (Figure 11). If the ULXs were all background and/or foreground objects, a random (i.e., flat) radial distribution would be expected. The observed radial distribution, therefore, implies that more ULXs within the D_{25} isophotes are truly associated with the galaxies than the ULXs between $1-2 \times D_{25}$. In the deep survey of the late-type galaxies, there are 79 detected ULXs, 15.7 contaminating sources, and 63.3 “true” ULXs within the D_{25} isophotes (Table 2), while there are 60 detected ULXs, 43.1 contaminating sources, and 16.9 “true” ULXs between $1-2 \times D_{25}$. Therefore the bulk of the “true” ULXs ($\sim 80\%$) is within the D_{25} isophotes. Note that 12 ULXs between $1-2 \times D_{25}$ are associated with dust loops/strips and spiral arms, and are apparently connected to the galaxies, which account for $\sim 70\%$ of the “true” ULXs.

The radial distribution of ULXs is more extended than the blue light in the late-type galaxies. The survey blue light per annulus peaks at $R \sim h$ if the light follows an exponential disk profile with a scale height of h as described in Section 2.3. In the deep survey for the late-type galaxies, this peak occurs at $0.3R_{25}$ since $\bar{h} = 0.3R_{25}$. In comparison, the number of ULXs per annulus peaks at $0.5R_{25}$, indicative of a higher scale height for the ULX distribution than that for the blue light (Figure 12). It is also suggested by the gradual increase in the number of ULXs per unit blue light with radii (Figure 13). This is expected since $\geq 75\%$ of the ULXs are on the spiral arms (Paper I), while the spiral arms are more extended than the light profile.

For the early-type galaxies, the detected ULXs are radially distributed as the predicted contaminating sources, except for a marginal excess of detected ULXs around $0.4R_{25}$ (Figure 14) that vanishes for ULXs above 2.5×10^{39} erg/sec. Finding that the ULX candidates in early-type galaxies in CP2002 are distributed randomly, Irwin et al. (2004) argue these candidates are contaminating sources, and they contend that there are no true ULXs above 2×10^{39} erg/sec in early-type galaxies. Indeed, there should be very few true ULXs in our survey of early-type galaxies: 10 ULX candidates are detected within the D_{25} isophotes with 10.3 contaminating sources predicted, and 32 ULXs are detected between $1-2 \times D_{25}$ with 29.7 contaminating sources predicted.

5. DISCUSSIONS

In this paper, statistical properties of the ULX populations constructed from our recent HRI survey of X-ray sources in nearby galaxies (Liu & Bregman, 2005) are studied with particular attention to the contamination problem. The ULXs as extranuclear X-ray point sources above 10^{39} erg/sec are found common in late-type galaxies. For example, $\sim 40\%$ of the late-type galaxies harbor at least one ULX with 0.84 ± 0.13 ULXs per $10^{10} L_{\odot}$ in our HRI survey. The luminosity functions of the X-ray source populations in different galaxy samples are analyzed to study the connection between HMXB/LMXBs and ULXs, and to reveal the dependence of ULXs on the star formation activities.

5.1. HMXB/LMXBs, regular ULXs and extreme ULXs

This HRI survey has a significant coverage at low luminosities, with X-ray sources of 2×10^{38} erg/sec detectable in $\sim 10\%$ of the total surveyed blue light. The luminosity functions, therefore, are studied in the luminosity range of $10^{38}-10^{41}$ erg/sec, which enables direct comparisons between the ordinary HMXB/LMXB populations and the ULX populations.

The luminosity functions of the HMXB/LMXBs and ULXs in the late-type galaxies can be fitted by a single power-law below 10^{40} erg/sec, with no breaks between the two populations. This is comparable to the work by Grimm et al. (2003), which shows that the X-ray source (mainly HMXBs) populations in 12 nearby starburst galaxies, as well as the Milky Way and Magellanic Clouds, follow the same universal luminosity function scaled by the star formation rate, i.e., $\frac{dN}{dL_{38}} = 3.3_{-0.8}^{+1.1} \text{SFR} L_{38}^{-1.61 \pm 0.12}$ for $L_c < 2 \times 10^{40}$ erg/sec, where L_{38} is the X-ray luminosity in units of 10^{38} erg/sec. The absence of breaks between the ordinary HMXB/LMXBs and the regular ULXs suggests that *the regular ULX population*

must be some kind of high luminosity extension of the ordinary HMXB/LMXB populations, all of which are associated with the same underlying distributions of primary masses, binary properties, and accretion rates. The HMXB-like ULXs could be stellar mass black hole binaries with high mass secondaries undergoing thermal timescale mass transfer through Roche lobe overflow (King et al. 2001), and the LMXB-like binaries could be the soft X-ray transients in their bright outburst phases (King et al. 2002).

The existence of a cutoff around 10^{40} erg/sec in the luminosity function can have significant implications for understanding the nature of ULXs. This cutoff, present both in Grimm et al. (2003) and in this work, suggests a cutoff of $\sim 100M_{\odot}$ in the mass distribution of black holes if the ULXs radiate at the canonical Eddington luminosity. If the mass distribution of black holes cuts off around $\sim 15M_{\odot}$, the most massive black hole achievable in the ordinary stellar evolution models, the ULXs must radiate at > 6 times the Eddington luminosity. These apparent super-Eddington radiation can result from many effects, such as beamed emission (King et al. 2001), emission of a jet (Kording et al. 2002), emission from a supercritical accretion disk (Shakura & Sunyaev 1973), or emission from a magnetized accretion disk where the photon-bubble instabilities operate (Begelman 2002).

The extreme ULXs above 10^{40} erg/sec might be a different population from the regular ULXs below 10^{40} erg/sec. This is evidenced by the flattening of the luminosity function of the extreme ULXs as compared to the luminosity function of the regular ULXs, and the significant ($\sim 2\sigma$) gap separating the two populations. For the ULX population in the late-type galaxies, seven extreme ULXs are detected, 1.5 contaminating sources are predicted, and 19.5 extreme ULXs are expected from the power-law fit for the regular ULXs. These numbers suggest that most of these extreme ULXs are “true” ULXs, and there are significantly ($\sim 3\sigma$) fewer extreme ULXs than the regular ULXs. The extreme ULXs are usually found in star-forming regions, and some have X-ray spectral features of systems with black holes of $\geq 1000M_{\odot}$, e.g., the ULX in Holmberg IX (Miller et al. 2004) and the ULX in NGC1313 (Miller et al. 2003). Thus it is reasonable to postulate that the extreme ULXs could be the intermediate mass black holes as suggested by Colbert & Mushotzky (1999), while the regular ULXs are systems of stellar mass black holes. There are, however, only a few extreme ULXs detected in the HRI survey, and larger surveys with more extreme ULXs are needed to study whether the extreme ULXs are a truly different population, and the details of the luminosity function.

There is no significant ULX population in the early-type galaxies in our HRI survey. In the early-type galaxies, the X-ray sources are dominated by LMXBs, and the luminosity function shows a cutoff at $\sim 10^{39}$ erg/sec, suggestive of a cutoff of $\sim 10M_{\odot}$ in the mass distribution of stellar mass black holes if they radiate at the Eddington luminosity. Such a

cutoff has been verified with Chandra observations of nearby elliptical galaxies M87, M49 and NGC4697 (Jordan et al. 2004). In the deep survey, 10 ULX candidates above 10^{39} are detected with 10.3 contaminating sources predicted from the $\log N$ – $\log S$ relation, and the two radial distributions are consistent with each other, indicative of absence of “true” ULXs in early-type galaxies. This is consistent with the claimed lack of ULXs above 2×10^{39} erg/sec in the 0.3–10 keV band in early-type galaxies (Irwin et al. 2004). The “true” ULXs in early-type galaxies, if present, cannot be explained by the thermal timescale mass transfer of HMXBs owing to the absence of high mass stars; instead they can be soft X-ray transients in their bright outburst phases (King et al. 2002).

5.2. Star formation and the ULX phenomenon

A close connection between the ULX phenomenon and star formation is revealed statistically in the HRI survey. This connection implies that ULXs preferentially occur in late-type galaxies than in early-type galaxies owing to the lack of star formation in the latter; it is indeed observed in the HRI survey. In the deep survey, there are 0.72 ± 0.10 ULXs per survey galaxy for the late-type galaxies, while only 0.02 ± 0.10 ULXs per survey galaxies for the early-type galaxies. We note that six of the ten ULX candidates in early-type galaxies are from the lenticular galaxies NGC1316 and NGC5128 with recent merging events and induced star formation activities. In late-type galaxies, ULXs preferentially occur on the spiral arms or dust lanes, with 75% (81/106) of the ULXs in the clean sample of Paper I in such regions. This may explain why the radial distribution of ULXs has a larger scale height than the light profile, since the spiral arms are more extended than the light. The ULXs outside the D_{25} isophotes consist of $\sim 20\%$ of all ULXs in late-type galaxies, and are also preferentially found in star forming regions, with about 70% associated with spiral arms or other dust regions. Among late-type galaxies, the starburst/HII galaxies with significant current star formation activities have higher ULX rates than the non-starburst galaxies. The close connection is further supported by a general increasing trend of the occurrence frequencies and ULX rates with the star formation rate.

The close connection between ULXs and star formation has been confirmed by recent optical observations with the Hubble Space Telescope and ground-based telescopes. Pakull & Mirioni (2002) observed 15 ULXs in 11 galaxies, and found 13 ULXs associated with well-defined HII regions and emission nebulae. In comparison, only a few ULXs are reported to associate with globular clusters, e.g., the ULX in NGC4565 (Wu et al. 2001), and the two ULXs in NGC1399 (Angelini et al. 2002). Such a connection is consistent with the postulation that ULXs are high-mass X-ray binary systems that are undergoing thermal

timescale mass transfer through Roche lobe overflow (King et al. 2002). Unlike the ordinary Galactic HMXBs that accrete by capturing the stellar winds, the accretion rates for these HMXB-like ULXs are high enough to power radiation at near/super Eddington luminosities. This HMXB scenario is directly supported by the optical identifications of some ULXs with high mass stars, i.e., the ULX in M81 with an O8 V star (Liu et al. 2002), and the ULX in NGC5204 with a B0 Ib supergiant (Liu et al. 2004).

In addition to HMXB-like ULXs, there must be LMXB-like ULXs in the late-type galaxies, since the HMXB-like ULXs alone cannot account for all the detected ULXs. The HMXBs trace the star formation activities for its short lifetime ($\sim 10^7$ years), and are expected to be linearly proportional to the star formation rate of a galaxy. Grimm et al. (2003) verified this linear relation with Chandra observations of nearby starburst galaxies, and found a universal luminosity function, i.e., $\frac{dN}{dL_{38}} = 3.3_{-0.8}^{+1.1} \text{SFR} L_{38}^{-1.61 \pm 0.12}$ for $L < 2 \times 10^{40}$ erg/sec, where L_{38} is the X-ray luminosity in units of 10^{38} erg/sec. If all ULXs are HMXB-like, a linear relation would be expected between the number of ULXs and the star formation rates. However, no such linear relation is found in this HRI survey, which includes galaxies with star formation rates from $< 0.001 M_{\odot}/yr$ to $17 M_{\odot}/yr$. Instead, a non-linear relation with the form $N(L_X > 10^{39}) = 7.0_{-1.9}^{+1.9} \text{SFR}^{0.36_{-0.10}^{+0.07}}$ is found for ULXs above 10^{39} erg/sec. For galaxies with low star formation rates ($< 0.4 M_{\odot}/yr$), the detected ULXs are significantly more than the HMXB-like ULXs expected from the linear relation. This excess of ULXs can be contributed as LMXBs, which are soft X-ray transients in their bright outburst phases as suggested by King et al. (2002).

The observed non-linear relation implies the fraction of HMXB-like ULXs increases with the star formation rate, which is expected since the LMXB-like ULXs trace the total mass/light instead of the star formation rate, thus its rate keeps constant while the total ULX rate increases with the star formation rate. We estimate that the total number of ULXs $N = 0.93\mathcal{L} + 0.20\text{SFR}$, with the surveyed light \mathcal{L} in unit of $10^{10} L_{\odot}$, and the star formation rate in unit of M_{\odot}/yr . While this relation correctly predicts the increase of the HMXB-like ULXs with the star formation rate, it cannot be taken quantitatively, since it severely underestimates the contribution of HMXB-like ULXs owing to the difference between HRI and ACIS in the X-ray spectral sensitivity and the source blending effects at large star formation rates. Chandra observations of galaxies with high star formation rates are needed to alleviate the blending effects to accurately quantify the relative fractions of HMXB-like ULXs and LMXB-like ULXs.

we are grateful to the NED, VizieR services. We would like to thank Renato Dupke, Eric Miller, Rick Rothschild, and Steven Murray for helpful discussions. We gratefully acknowledge support for this work from NASA under grants HST-GO-09073.

REFERENCES

- Angelini, L., Loewenstein, M., and Mushotzky, R.F., 2001, ApJL, 557, 35
- Bauer, F.E., Brandt, W.N., Sambruna, R.M., Chartas, G., Garmire, G.P., Kaspi, S., and Netzer, H., 2001, AJ, 122, 182
- Begelman, M.C., 2002, ApJ, 568, L97
- Bell, E., and de Jong, R., 2001, ApJ, 550, 212
- Colbert, E. J. M. and Mushotzky, R. F. 1999, ApJ, 519, 89
- Colbert, E. and Ptak, A. 2002, ApJS, 143,25
- Colbert, E., Heckman, T., Ptak, A., and Strickland, D., 2004, ApJ, 602, 231
- de Vaucouleurs, G., de Vaucouleurs, A., Corwin, H., Buta, R., Paturel, G., and Fouque, P, 1991, *Third Reference Catalogue of Bright Galaxies*
- Fabbiano, G. 1989, ARA&A, 27, 87
- Gao, Y., Wang, Q., Appleton, P., and Lucas, R., 2003, ApJL, 596, 171
- Graham, A., 2001, AJ, 121, 820
- Grimm, H., Gilfanov, M., and Sunyaev, R., 2003, MNRAS, 339, 793
- Hasinger, G., Burg, R., Giacconi, R., Schmidt, M., Trumper, J. and Zamorani, G. . 1998, A&A, 329, 482
- Irwin, J., Bregman, J., and Athey, A., 2004, ApJL, 60, 143
- Jordan, A, Cote, P., Ferrarese, L., Blakeslee, J., et al. 2004, ApJ, 613, 279
- Liu, J., and Bregman, J., 2005, ApJS, in press
- Liu, J., Bregman, J., Lloyd-Davies, E., Irwin, J., Espaillat, C., and Seitzer, P., 2004, submitted
- Liu, J., Bregman, J., and Seitzer, P., 2002, ApJL, 580, 31
- Liu, J., Bregman, J., and Irwin, J., 2002, ApJL, 581, 93
- Kilgard, R., Kaaret, P., Krauss, M., Prestwich, A., Raley, M., and Zezas, A., 2002, ApJ, 573, 138

- King, A.R., Davies, M.B., Ward, M.J., Fabbiano, G., and Elvis, M. 2001, *ApJ*, 552, L109
- King, A.R., 2002, *MNRAS*, 335, 513
- Kording, E., Falcke, H., Markoff, S., 2002, *A&A*, 382, L13
- Makishima, K., Kubota, A., Muzuno, T., Ohnishi, T., Tashiro, M., et al. 2000, *ApJ*, 535, 632
- Miller, J., Fabbiano, G., Miller, M., and Fabian, A., 2003, *ApJ*, 585, 37
- Miller, J., Fabian, A., and Miller, M., 2004, *ApJ*, 607, 931
- Pakull, M.W. and Mirioni, L., 2002, *astro-ph/0202488*
- Ptak, A., and Colbert, E., 2004, *ApJ*, 606, 291
- Rice, W., Lonsdale, C, Soifer, B., Neugebauer, G., Koplan, E., Lloyd, L., de Jong, T., and Habing, H., 1988, *ApJS*, 68, 91
- Roberts, T. P. and Warwick, R. S. 2000, *MNRAS*, 315, 98 (RW2000)
- Rosa-Gonzalez D., , Terlevich, E., and Terlevich, R., 2002, *MNRAS*, 332, 283
- Shakura, N., and Sunyaev, R., 1973, *A&A*, 24, 337
- Soria, R., and Motch, C., 2004, *A&A*, 422, 915
- Soria, R., Motch, C., Read, A., and Stevens, I, 2004, *A&A*, 423, 955
- Strohmayer, T., and Mushotzky, R., 2003, *ApJL*, 586, 61L
- Sugiho, M., Kotoku, J., Makishima, K., Kubota, A., Mizuno, T., Fukazawa, Y., and Tashiro, M. 2001, *ApJ*, 561, L73
- Swartz, D., Ghosh, K., Tennant, A., and Wu, K., 2004, *ApJS*, 154, 519
- Wu, H., Xue, S., Xia, X., Deng, Z., and Mao, S., 2002, *ApJ*, 576, 738
- Zezas, A., Fabbiano, G., Rots, A., and Murray, S., 2002, *ApJS*, 142, 239

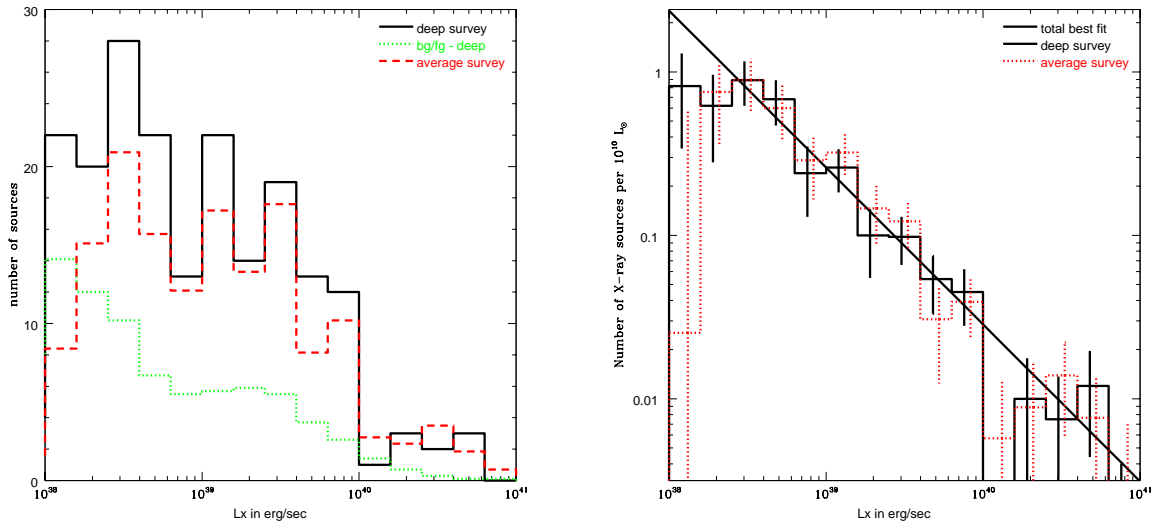


Fig. 1.— The luminosity functions for the X-ray source population in all galaxies in the deep survey and in the average survey. (left) Histograms of the numbers of detected ULXs (solid) and contaminating sources (dotted) in the deep survey, and detected ULXs in the average survey (dashed). (right) The luminosity functions scaled by the survey blue light for the deep survey (solid) and for the average survey (dotted) are plotted in histograms, with the power-law fit for the deep survey (solid) overplotted for comparison.

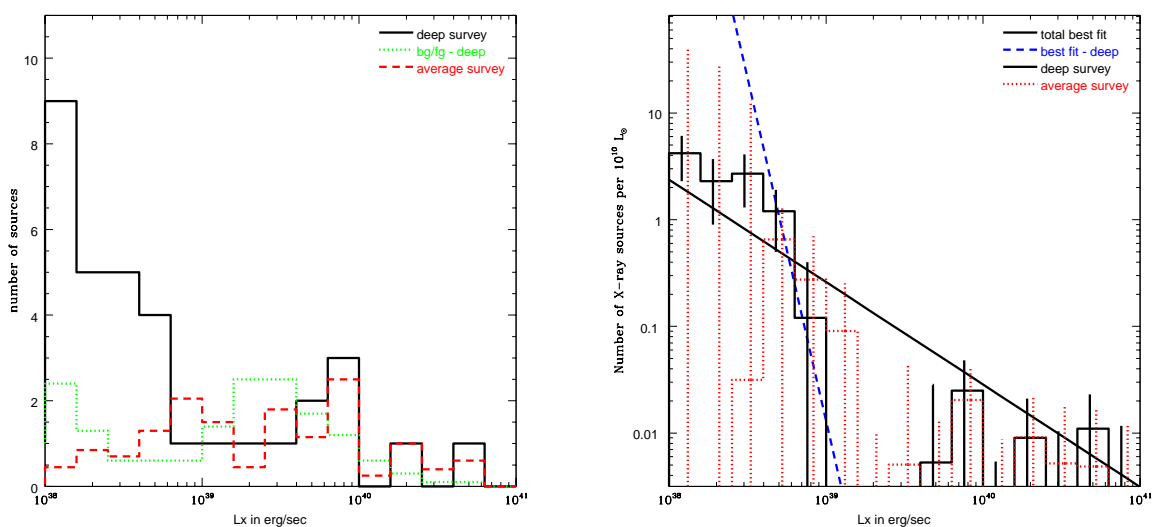


Fig. 2.— The luminosity functions for the X-ray source population in the early-type galaxies in the deep survey and in the average survey. (left) Histograms of the numbers of detected ULXs (solid) and contaminating sources (dotted) in the deep survey, and detected ULXs in the average survey (dashed). (right) The luminosity functions scaled by the survey blue light for the deep survey (solid) and for the average survey (dotted) are plotted in histograms, with the power-law fit to the total X-ray population in all galaxies (solid) and the power-law fit to the X-ray population in the early-type galaxies (dashed) overplotted for comparison.

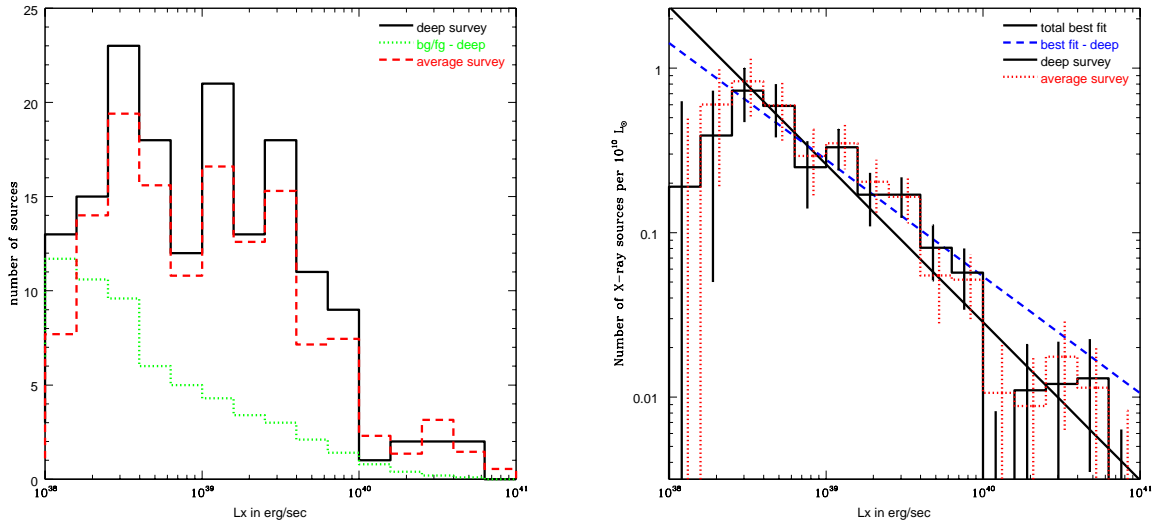


Fig. 3.— The luminosity functions for the X-ray source populations in the late-type galaxies in the deep survey and in the average survey. (left) Histograms of the numbers of detected ULXs (solid) and contaminating sources (dotted) in the deep survey, and detected ULXs in the average survey (dashed). (right) The luminosity functions scaled by the survey blue light for the deep survey (solid) and for the average survey (dotted) are plotted in histograms, with the power-law fit to the total X-ray source population in all galaxies (solid) and the power-law fit to the X-ray source population in the late-type galaxies (dashed) overplotted for comparison.

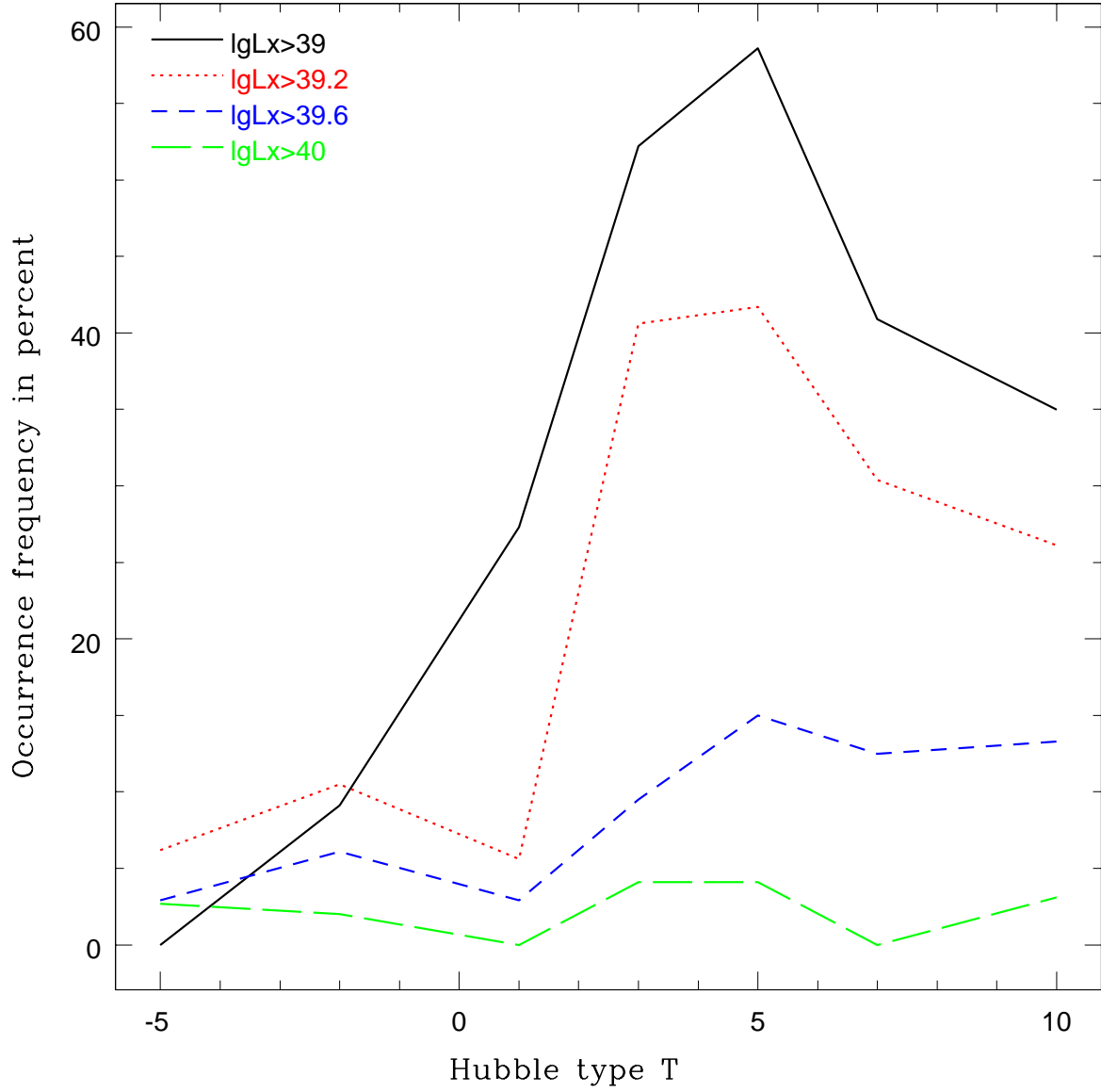


Fig. 4.— The occurrence frequencies as a function of the Hubble type T of galaxies for ULXs above $1/1.6/4.0/10 \times 10^{39}$ erg/sec.

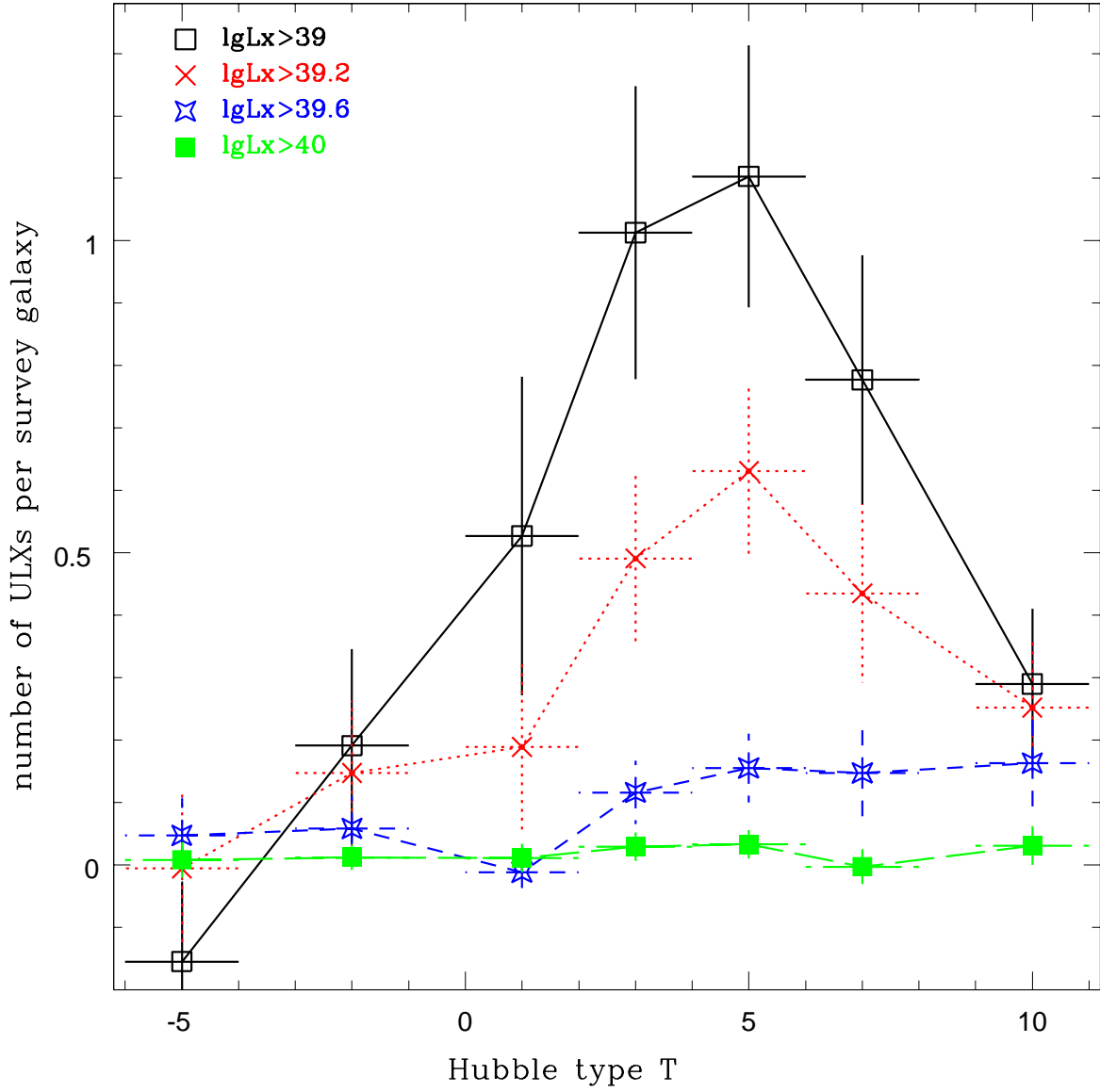


Fig. 5.— The net numbers of ULXs per survey galaxy as a function of the Hubble type T of galaxies for ULXs above $1/1.6/4.0/10 \times 10^{39}$ erg/sec.

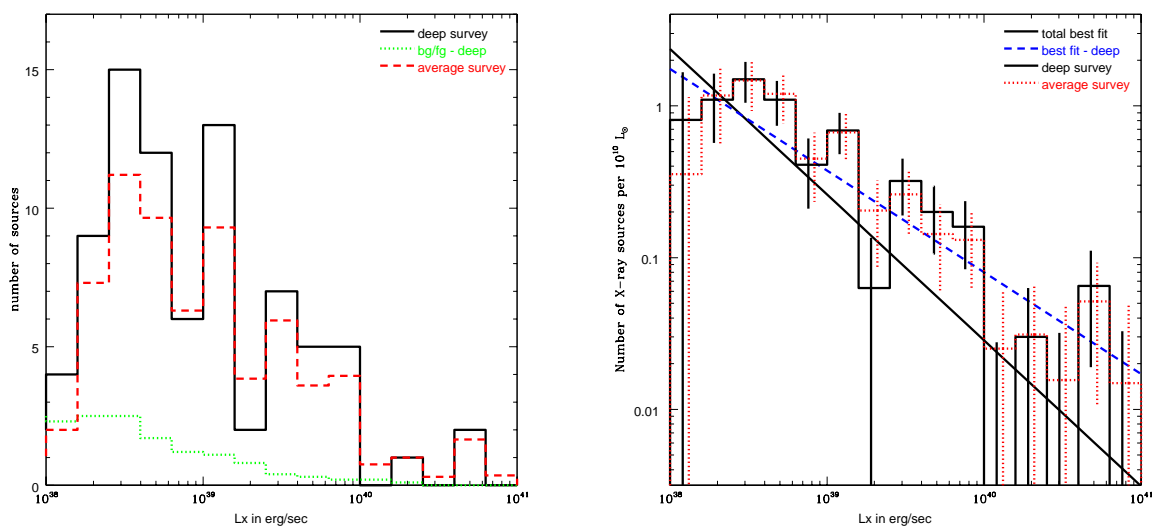


Fig. 6.— The luminosity functions for the X-ray source populations in the starburst/HII galaxies in the deep survey and in the average survey. (left) Histograms of the numbers of detected ULXs (solid) and contaminating sources (dotted) in the deep survey, and detected ULXs in the average survey (dashed). (right) The luminosity functions scaled by the survey blue light for the deep survey (solid) and for the average survey (dotted) are plotted in histograms, with the power-law fit to the total X-ray population in all galaxies (solid) and the power-law fit to the X-ray population in the starburst/HII galaxies (dashed) overplotted for comparison.

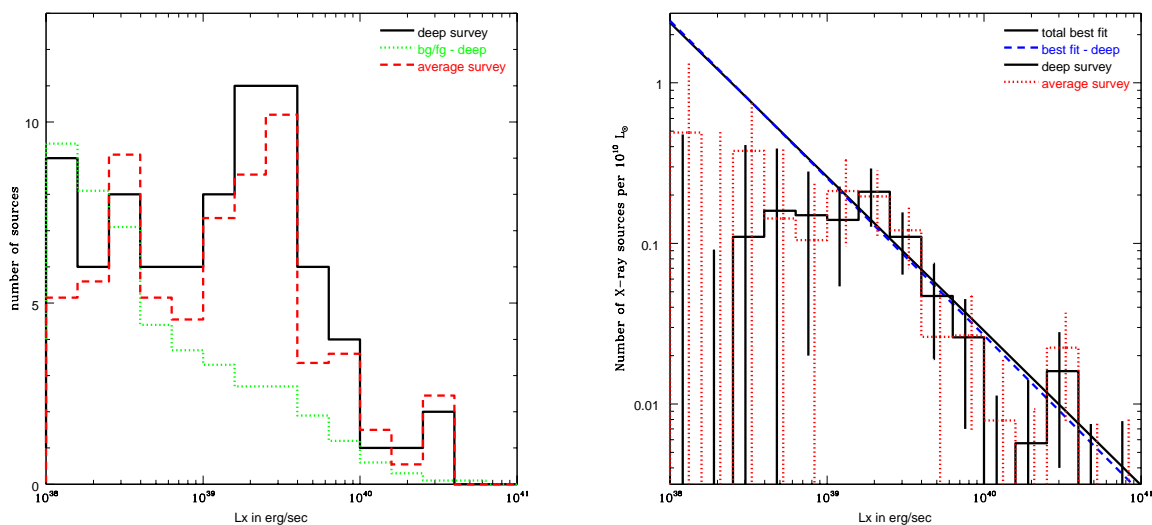


Fig. 7.— The luminosity functions for the X-ray source populations in the non-starburst late-type galaxies in the deep survey and in the average survey. (left) Histograms of the numbers of detected ULXs (solid) and contaminating sources (dotted) in the deep survey, and detected ULXs in the average survey (dashed). (right) The luminosity functions scaled by the survey blue light for the deep survey (solid) and for the average survey (dotted) are plotted in histograms, with the power-law fit to the total X-ray population in all galaxies (solid) and the power-law fit to the X-ray population in the non-starburst late-type galaxies (dashed) overplotted for comparison.

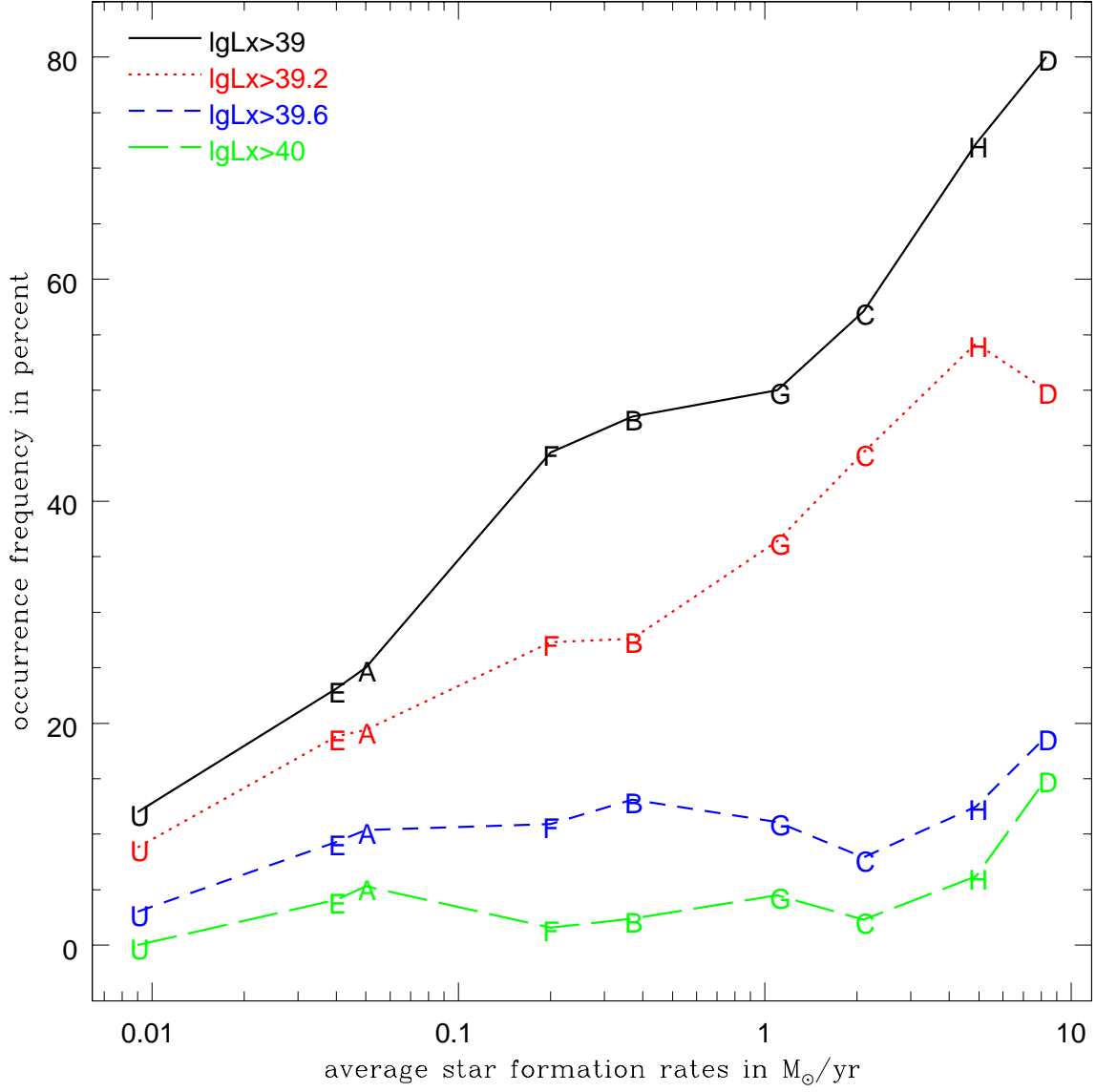


Fig. 8.— The occurrence frequencies as a function of the star formation rates of galaxies for ULXs above $1/1.6/4.0/10 \times 10^{39}$ erg/sec.

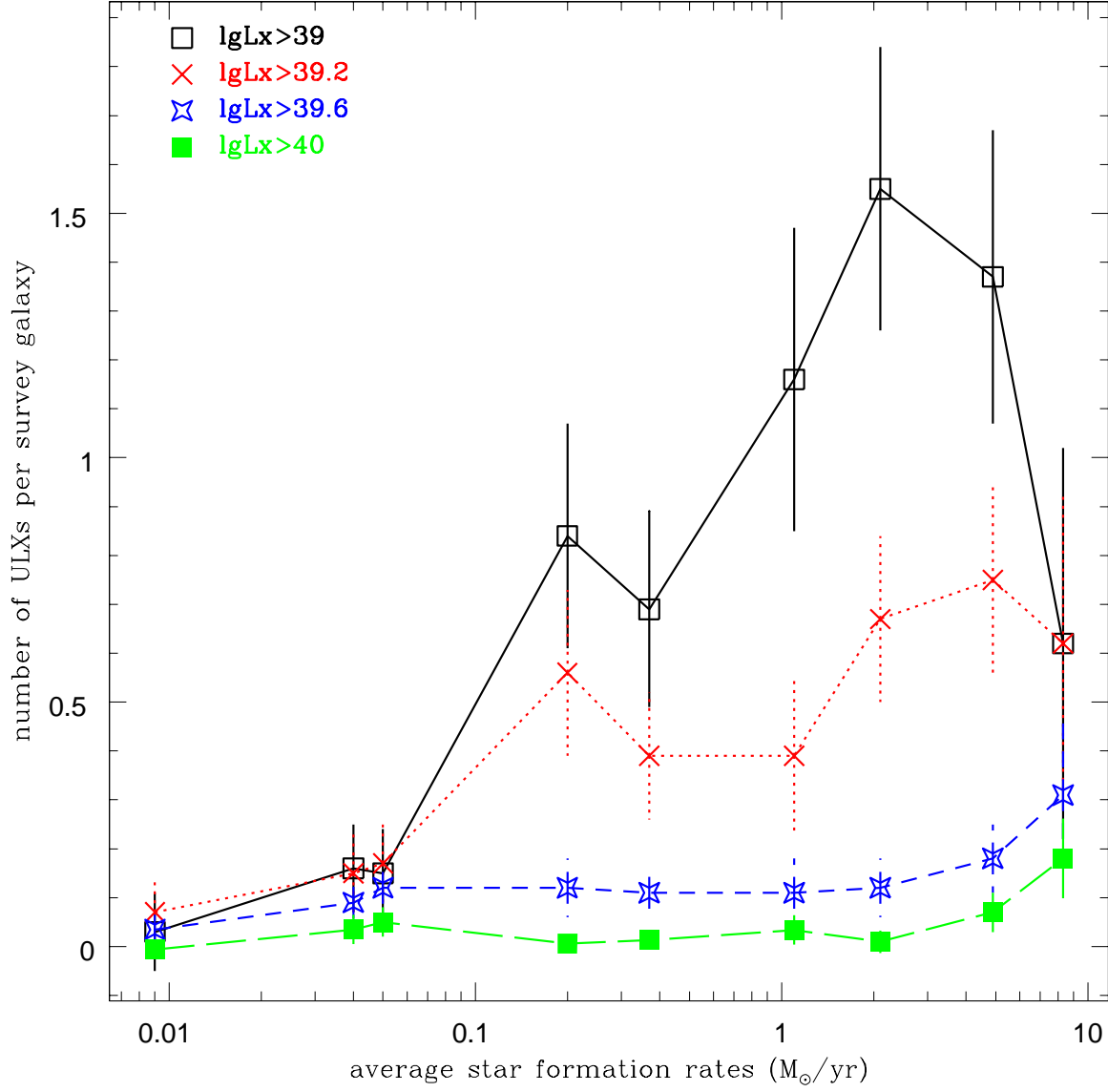


Fig. 9.— The net numbers of ULXs per survey galaxy as a function of the star formation rates of galaxies for ULXs above $1/1.6/4.0/10 \times 10^{39}$ erg/sec.

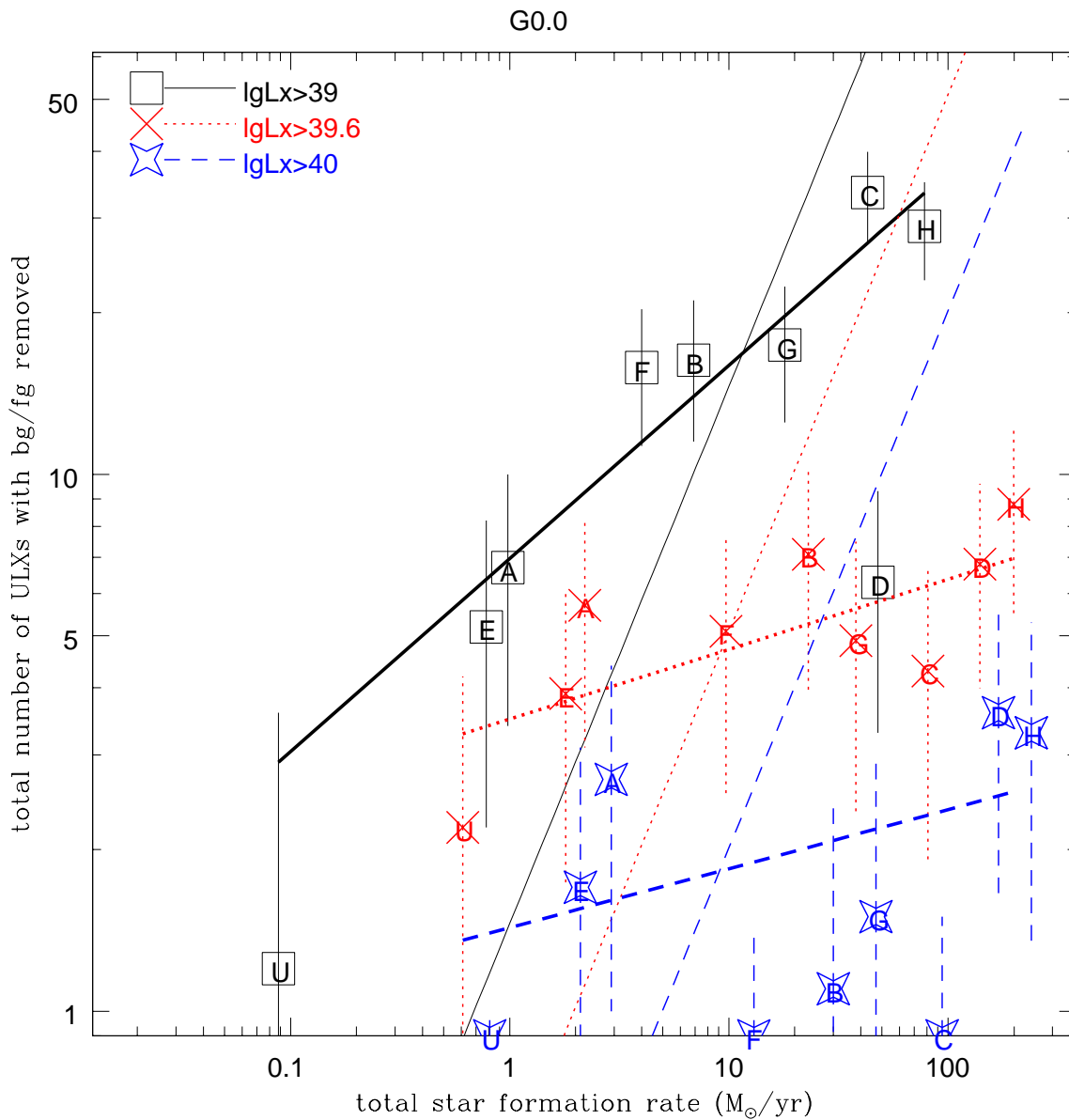


Fig. 10.— The numbers of ULXs in a group of galaxies as a function of total star formation rates. The fitted power-law functions are plotted in thick lines, with the N_{ULX} – SFR relation from Grimm et al. (2003) overplotted in thin lines for comparison.

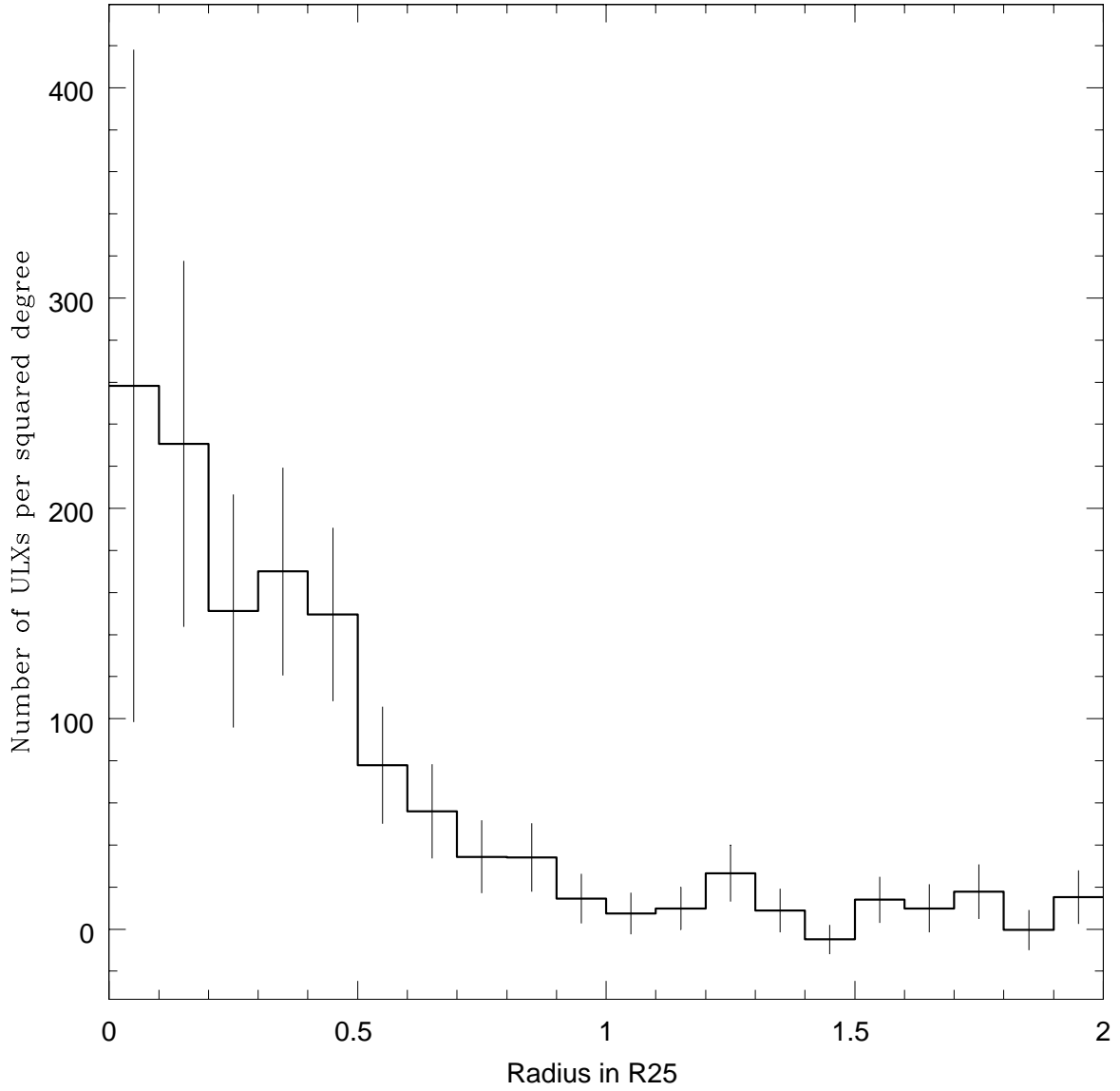


Fig. 11.— The surface number density of ULXs in the late-type galaxies. The contaminating sources predicted with the $\log N$ – $\log S$ relation are subtracted from the detected ULXs.

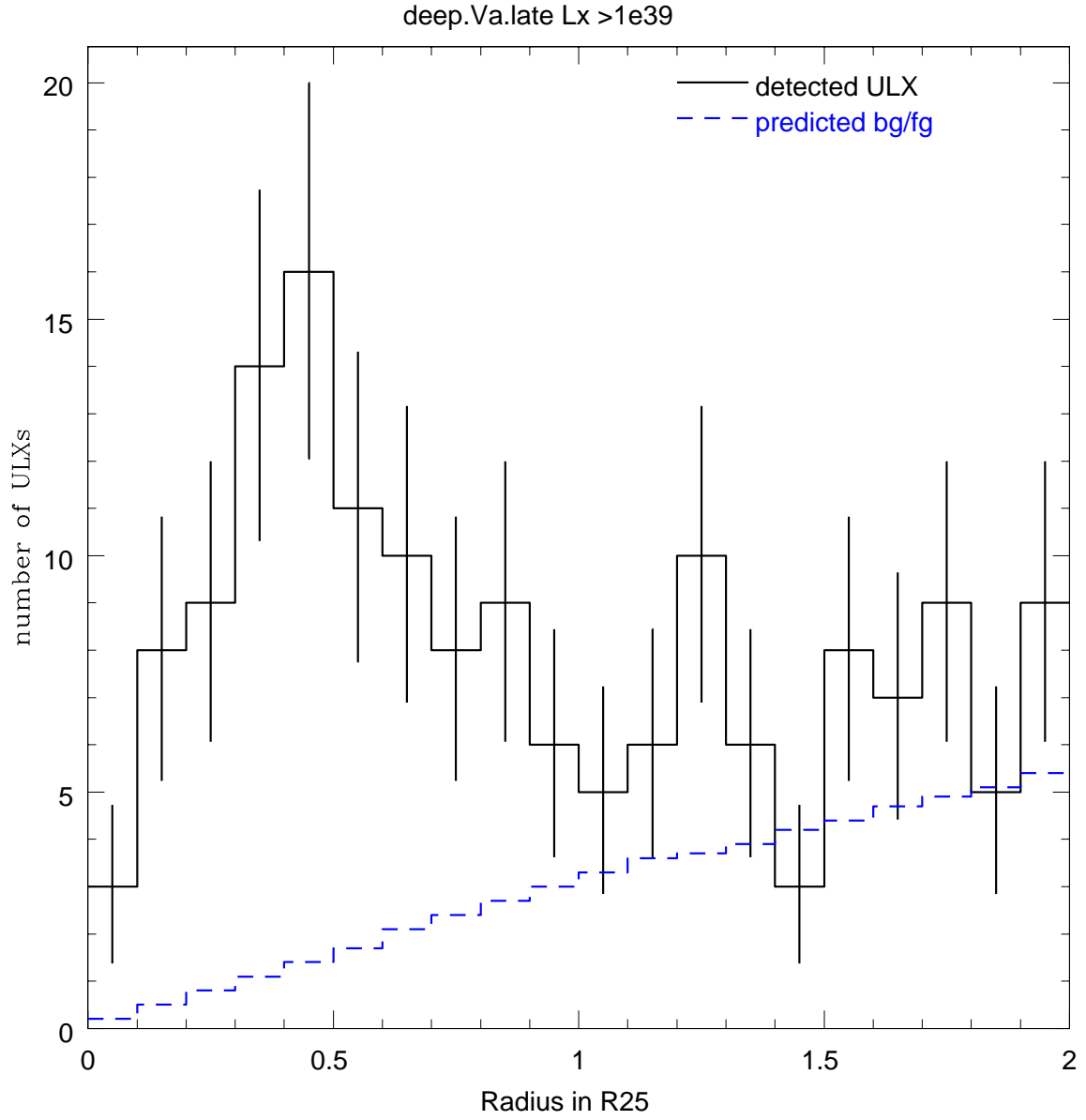


Fig. 12.— The radial distribution of detected ULXs and predicted contaminating sources above 10^{39} erg/sec in the late-type galaxies.

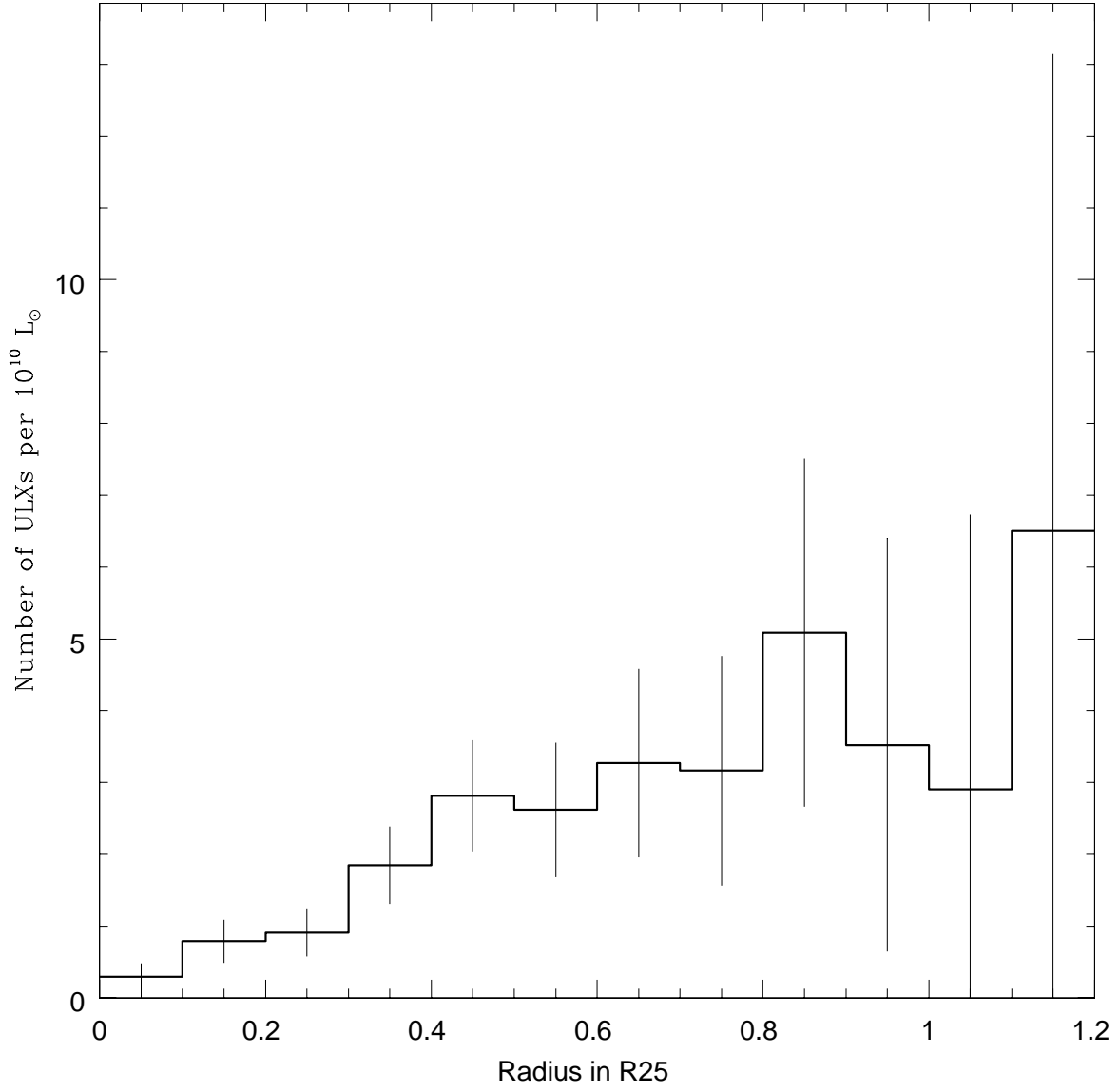


Fig. 13.— The number of ULXs per unit blue light in the late-type galaxies. The contaminating sources predicted with the $\log N$ – $\log S$ relation are subtracted from the detected ULXs.

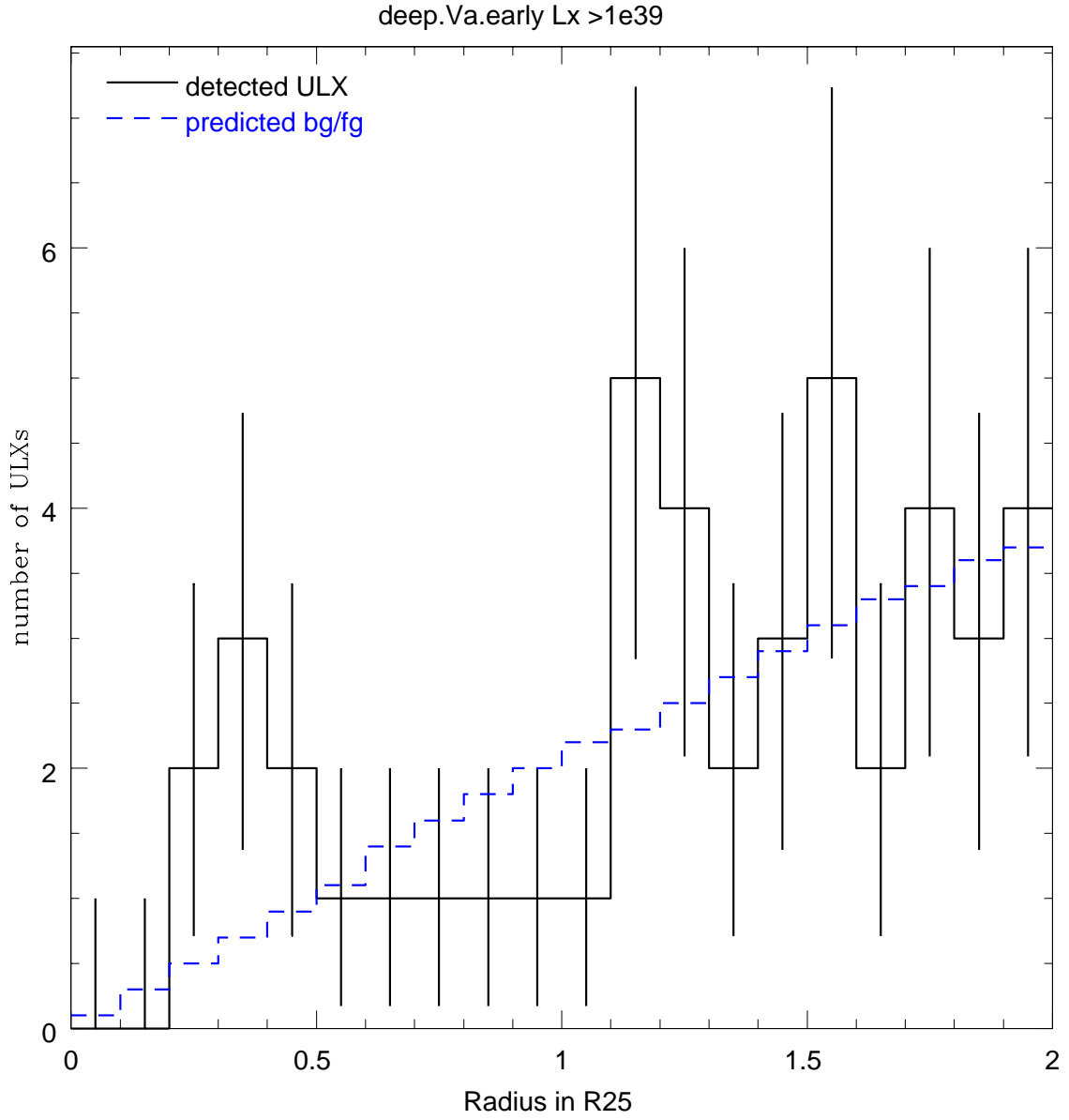


Fig. 14.— The radial distribution of detected ULXs and predicted contaminating sources above 10^{39} erg/sec in the early-type galaxies.

Table 1. ULX occurrence rates for different survey galaxy samples

sample ^a	$L_X \geq 10^{39}$ erg/sec ^b					$L_X \geq 1.6 \times 10^{39}$ erg/sec ^c					$L_X \geq 4.0 \times 10^{39}$ erg/sec ^d					$L_X \geq 10^{40}$ erg/sec ^e				
	98	35	35.7	1.71±0.23	0.56±0.09	131	33	25.2	1.40±0.21	0.32±0.06	226	20	8.8	1.20±0.25	0.10±0.025	281	8	2.8	0.99±0.35	0.02
all	98	35	35.7	1.71±0.23	0.56±0.09	131	33	25.2	1.40±0.21	0.32±0.06	226	20	8.8	1.20±0.25	0.10±0.025	281	8	2.8	0.99±0.35	0.02
early	22	1	4.5	1±1	0.023±0.10	35	3	8.6	1.07±0.67	0.08±0.09	67	3	4.5	1.40±0.73	0.05±0.04	88	2	2.3	1±0.70	0.01
earlyx	21	1	4.8	1±1	-0.019±0.10	33	2	6.1	1.10±0.85	0.036±0.07	65	2	3.1	1.40±0.85	0.03±0.034	86	2	2.3	1±0.70	0.012
late	76	34	44.7	1.73±0.23	0.72±0.10	96	30	31.2	1.43±0.22	0.41±0.07	159	17	10.7	1.16±0.27	0.12±0.03	193	6	3.1	0.98±0.40	0.03
pec	3	0	0	0±0	-0.033±0.33	3	0	0	0±0	-0±0.33	4	0	0	0±0	-0.025±0.25	4	0	0	0±0	-
ellip	11	0	0	0±0	-0.155±0.13	16	1	6.2	1.20±1.40	-0.006±0.12	34	1	2.9	1.80±1.40	0.05±0.06	37	1	2.7	1±1	0.008
lent	11	1	9.1	1±1	0.19±0.15	19	2	10.5	0.95±0.70	0.15±0.12	33	2	6.1	1.20±0.85	0.06±0.05	51	1	2	1±1	0.01
lentx	10	1	10	1±1	0.12±0.14	17	1	5.9	1±1	0.08±0.08	31	1	3.2	1±1	0.016±0.03	49	1	2	1±1	0.01
Sa	11	3	27.3	1.53±0.73	0.53±0.26	18	1	5.6	1±1	0.19±0.13	34	1	2.9	1±1	-0.012±0.03	44	0	0	0±0	0.01
Sb	23	12	52.2	1.93±0.42	1.01±0.23	32	13	40.6	1.44±0.35	0.49±0.14	63	6	9.5	1.15±0.43	0.12±0.05	73	3	4.1	1±0.57	0.03
Sc	29	17	58.6	2.09±0.36	1.10±0.21	36	15	41.7	1.72±0.35	0.63±0.14	60	9	15	1.20±0.37	0.15±0.06	73	3	4.1	0.97±0.57	0.03
Sd	22	9	40.9	1.86±0.47	0.78±0.20	23	7	30.4	1.40±0.46	0.43±0.14	32	4	12.5	1±0.50	0.15±0.07	36	0	0	0±0	-0.00
Sm	20	7	35	1.13±0.40	0.29±0.12	23	6	26.1	1.15±0.43	0.25±0.10	30	4	13.3	1.25±0.55	0.16±0.07	32	1	3.1	1±1	0.0
Sbrst	26	18	69.2	1.81±0.32	0.98±0.20	29	15	51.7	1.37±0.31	0.53±0.14	40	10	25	1.19±0.35	0.26±0.08	46	2	4.3	1±0.70	0.0
nSbrstL	52	16	30.8	1.65±0.34	0.56±0.12	70	15	21.4	1.51±0.33	0.34±0.08	123	7	5.7	1.11±0.40	0.07±0.03	152	4	2.6	0.97±0.50	0.018
SFRU	25	3	12	1.30±0.67	0.03±0.08	34	3	8.8	1.40±0.73	0.07±0.07	66	2	3	1.90±1	0.035±0.03	83	0	0	0±0	-0.006
SFRA	28	7	25	0.99±0.37	0.15±0.09	36	7	19.4	0.99±0.37	0.17±0.08	48	5	10.4	1±0.44	0.12±0.05	57	3	5.3	1±0.57	0.0
SFRB	21	10	47.6	1.53±0.40	0.69±0.20	29	8	27.6	1.46±0.44	0.39±0.13	61	8	13.1	1.04±0.38	0.11±0.05	82	2	2.4	1±0.70	0.013
SFRC	21	12	57.1	2.38±0.47	1.55±0.29	27	12	44.4	1.50±0.37	0.67±0.17	38	3	7.9	0.97±0.57	0.12±0.06	44	1	2.3	1±1	0.01
SFRD	5	4	80	1.52±0.65	0.62±0.40	8	4	50	1.60±0.65	0.62±0.30	16	3	18.8	1.63±0.73	0.31±0.15	20	3	15	0.97±0.57	0.1
SFRE	26	6	23.1	0.98±0.40	0.16±0.09	32	6	18.8	0.98±0.40	0.15±0.08	43	4	9.3	1±0.50	0.09±0.05	49	2	1.6	1±0.70	0.03
SFRF	18	8	44.4	1.66±0.46	0.84±0.23	22	6	27.3	1.62±0.53	0.56±0.17	46	5	10.9	0.98±0.44	0.12±0.06	63	1	1.6	1±1	0.006
SFRG	14	7	50	2.27±0.59	1.16±0.31	22	8	36.4	1.43±0.44	0.39±0.16	36	4	11.1	1.10±0.55	0.11±0.07	44	2	4.5	1±0.70	0.03
SFRH	18	13	72.2	1.97±0.41	1.37±0.30	24	13	54.2	1.45±0.35	0.75±0.19	40	5	12.5	1.36±0.52	0.18±0.07	48	3	6.2	0.97±0.57	0.0

^aThe survey galaxy sample. A 'x' is suffixed when the two peculiar lenticulars NGC1316 and NGC5128 are excluded from the early-type and lenticular sample.

^bFor ULXs with $L_X \geq 10^{39}$ erg/sec. The five numbers are, (1) the number of galaxies with survey light $\geq 0.1 \times$ its total light, (2) the number of galaxies with at least 0.5 net ULXs, (3) the fraction (%) of survey galaxies that host ULXs (4) the net ULXs per host galaxy, (6) the net ULXs per survey galaxy.

^bFor ULXs with $L_X \geq 1.6 \times 10^{39}$ erg/sec.

^bFor ULXs with $L_X \geq 4.0 \times 10^{39}$ erg/sec.

^bFor ULXs with $L_X \geq 10^{40}$ erg/sec.

Table 2. ULX rates for different survey galaxy samples

sample ^a	NG ^b	Lg ^c	$lgL_X = [39, 39.2]$									$lgL_X = [39.2, 39.4]$				
			ULX ^d	bg ^e	Net ^f	CNet ^g	SL/SFR ^h	Urate ⁱ	Crate ^j	ULX	bg	Net	CNet	SL/SFR	Urate	
all	296	0.78	22/89	5.7/26	16.3±4.7	63±9.4	59/95	0.26±0.08	0.59±0.10	14/67	5.9/20.3	8.1±3.7	46.7±8.2	91/130	0.1±0.045	0.3
early	91	0.9	1/10	1.4/10.3	-0.4±1	-0.3±3.2	9.5/2.2	-0.079±0.07	-0.13±0.09	1/9	2.5/8.9	-1.5±1	0.1±3	28/3.6	-0.062±0.026	-0.04
earlyx	89	0.8	1/7	1.4/8.8	-0.4±1	-1.8±2.6	8.0/0.5	-0.1±0.08	-0.19±0.09	0/6	2.2/7.4	-2.2±1	-1.4±2.4	23/1.3	-0.092±0.04	-0.08
late	205	0.74	21/79	4.3/15.7	16.7±4.6	63.3±8.9	49/93	0.33±0.09	0.84±0.13	13/58	3.4/11.4	9.6±3.6	46.6±7.6	63/120	0.17±0.06	0.5
pec	5	0.52	0/0	0/0.1	-0±1	-0.1±1	1.3/15	-0.03±0.75	-0.076±0.39	0/0	0/0.1	-0±1	-0.1±1	1.3/15	-0.014±0.75	-0.04
ellip	38	1.4	0/4	1.1/7.2	-1.1±1	-3.2±2	5.5/0.1	-0.22±0.25	-0.34±0.04	0/4	1.9/6.1	-1.9±1	-2.1±2	20/0.4	-0.094±0.04	-0.1
lent	53	0.52	1/6	0.3/3.1	0.7±1	2.9±2.4	4.4/2.1	0.1±0.17	0.19±0.21	1/5	0.6/2.8	0.4±1	2.2±2.2	8.8/3.2	0.000±0.07	0.0
lentx	51	0.33	1/3	0.3/1.6	0.7±1	1.4±1.7	2.9/0.4	0.13±0.24	0.23±0.33	0/2	0.3/1.3	-0.3±1	0.7±1.4	4.3/0.9	-0.073±0.24	0.1
Sa	45	0.8	2/9	1/4.8	1±1.4	4.2±3	10/4.4	0.10±0.13	0.28±0.19	3/7	1.1/3.8	1.9±1.7	3.2±2.6	16/18	0.15±0.12	0.1
Sb	77	1.2	9/35	2.7/9.8	6.3±3	25.2±5.9	27/50	0.22±0.1	0.56±0.14	6/26	2/7.1	4±2.4	18.9±5.1	35/68	0.12±0.07	0.3
Sc	75	0.94	13/43	2.3/7.1	10.7±3.6	35.9±6.6	24/36	0.42±0.14	1±0.2	5/30	1.6/4.7	3.4±2.2	25.3±5.5	30/53	0.12±0.08	0.5
Sd	40	0.35	8/20	0.9/2.1	7.1±2.8	17.9±4.5	8.9/18	0.78±0.32	1.8±0.45	2/12	0.5/1.2	1.5±1.4	10.8±3.5	9.9/18	0.15±0.14	0.1
Sm	36	0.077	2/9	0.1/0.4	1.9±1.4	8.6±3	1.2/0.4	1.4±1.1	4.8±1.8	2/7	0.1/0.3	1.9±1.4	6.7±2.6	1.4/0.5	1.4±1	3
Sbrst	46	0.66	13/35	1.1/3.1	11.9±3.6	31.9±5.9	17/45	0.69±0.21	1.5±0.29	2/22	0.8/2	1.2±1.4	20±4.7	19/48	0.06±0.07	0.
nSbrstL	164	0.75	8/44	3.3/13.1	4.7±2.8	30.9±6.6	32/48	0.14±0.09	0.57±0.13	11/36	2.7/9.8	8.3±3.3	26.2±6	44/77	0.21±0.08	0.
SFRU	88	0.37	1/6	0.9/4.8	0.1±1	1.2±2.4	5.1/0.09	-0.084±0.11	-0.083±0.16	1/5	1.2/3.9	-0.2±1	1.1±2.2	11/0.14	-0.013±0.09	0.00
SFRA	60	0.57	0/11	0.8/4.3	-0.8±1	6.7±3.3	7.0/1.0	-0.11±0.12	0.16±0.14	1/11	1.2/3.5	-0.2±1	7.5±3.3	16/1.5	0.01±0.08	0.2
SFRB	88	0.79	5/23	1/6.7	4±2.2	16.3±4.8	14/6.9	0.28±0.16	0.65±0.21	5/18	1.3/5.7	3.7±2.2	12.3±4.2	22/11	0.21±0.12	0.3
SFRC	45	1.4	16/41	2.6/7.5	13.4±4	33.5±6.4	27/43	0.47±0.14	0.96±0.19	6/25	1.8/4.8	4.2±2.4	20.2±5	33/56	0.13±0.07	0.4
SFRD	20	1.7	0/9	0.3/2.7	-0.3±1	6.3±3	5.9/48	-0.057±0.18	0.25±0.18	1/9	0.4/2.4	0.6±1	6.6±3	9.7/64	0.10±0.14	0.
SFRE	51	0.56	0/9	0.8/3.8	-0.8±1	5.2±3	6.8/0.8	-0.12±0.13	0.14±0.15	1/9	1/3	-0±1	6±3	14/1.1	0.01±0.08	0.2
SFRF	68	0.69	5/20	0.8/4.2	4.2±2.2	15.8±4.5	10/4	0.38±0.21	0.99±0.29	5/15	0.8/3.4	4.2±2.2	11.6±3.9	14/4.6	0.34±0.18	0.
SFRG	46	1.1	8/24	1.3/6.6	6.7±2.8	17.4±4.9	13/18	0.49±0.2	0.8±0.24	4/16	1.5/5.3	2.5±2	10.7±4	24/25	0.13±0.1	0.3
SFRH	49	1.5	10/36	2/7	8±3.2	29±6	24/78	0.3±0.12	0.77±0.17	4/26	1.4/4.9	2.6±2	21.1±5.1	29/100	0.10±0.07	0.4

^aThe survey galaxy sample. A 'x' is suffixed when the two peculiar lenticulars NGC1316 and NGC5128 are excluded from the early-type and lenticular sample.

^bNumber of galaxies in this sample.

^cThe average blue light per galaxy in $10^{10} L_{\odot}$.

^dnumber of extra-nuclear X-ray sources observed in this bin, and the cumulative number.

^enumber of predicted background/foreground X-ray sources that would have luminosity in this bin, and the cumulative number

^fthe net number of X-ray sources in this bin, with errors as $\sqrt{N_{ULX}}$.

^gthe cumulative net number of X-ray sources with luminosity of this bin and larger.

^hsurveyed blue light in unit of $10^{10} L_{\odot}$ and the total star formation rates in M_{\odot}/yr for the luminosity in this bin.

ⁱthe ULX rate in unit of ULX per $10^{10} L_{\odot}$ in this bin.

^jthe ULX rate (ULX per $10^{10} L_{\odot}$) for luminosities in this bin and larger.

Table 3. ULX rates for different survey galaxy samples

sample ^a	NG ^b	Lg ^c	$lgL_X = [39.6, 39.8]$									$lgL_X = [40, 40.2]$				
			ULX ^d	bg ^e	Net ^f	CNet ^g	SL/SFR ^h	Urate ⁱ	Crate ^j	ULX	bg	Net	CNet	SL/SFR	Urate	Crate
all	296	0.78	13/34	3.7/9	9.3±3.6	25±5.8	170/250	0.05±0.02	0.13±0.03	1/9	1.4/2.6	-0.4±1	6.4±3	219/290	-0.002±0.004	0.03±0.0
early	91	0.9	2/7	1.7/3.9	0.3±1.4	3.1±2.6	60/6	0.005±0.023	0.04±0.04	0/2	0.6/1.1	-0.6±1	0.9±1.4	79/17	-0.008±0.013	0.01±0.0
earlyx	89	0.8	1/5	1.3/3.4	-0.3±1	1.6±2.2	49/3.6	-0.008±0.018	0.02±0.035	0/2	0.5/1	-0.5±1	1±1.4	69/15	-0.008±0.014	0.014±0.0
late	205	0.74	11/27	2.1/5	8.9±3.3	22±5.2	110/240	0.08±0.03	0.17±0.04	1/7	0.8/1.5	0.2±1	5.5±2.6	139/270	0.001±0.007	0.04±0.0
pec	5	0.52	0/0	0/0.1	-0±1	-0.1±1	1.7/26	-0.007±0.75	-0.026±0.39	0/0	0/0	-0±1	-0±1	2.6/26	-0.005±0.39	-0.009±0.0
ellip	38	1.4	1/4	1.1/2.7	-0.1±1	1.3±2	40/1.4	-0.005±0.02	0.023±0.04	0/1	0.4/0.8	-0.4±1	0.2±1	53/1.7	-0.008±0.02	0.005±0.0
lent	53	0.52	1/3	0.6/1.3	0.4±1	1.7±1.7	19/4.5	0.024±0.05	0.07±0.08	0/1	0.2/0.4	-0.2±1	0.6±1	26/16	-0.007±0.04	0.023±0.0
lentx	51	0.33	0/1	0.2/0.7	-0.2±1	0.3±1	9.2/2.2	-0.026±0.1	0.004±0.06	0/1	0.1/0.2	-0.1±1	0.8±1	15/13	-0.008±0.06	0.045±0.0
Sa	45	0.8	1/2	0.7/1.6	0.3±1	0.4±1.4	28/56	0.007±0.03	0.008±0.04	0/1	0.3/0.5	-0.3±1	0.5±1	35/68	-0.007±0.03	0.015±0.0
Sb	77	1.2	5/11	1.3/3.1	3.7±2.2	7.9±3.3	69/150	0.05±0.03	0.1±0.04	0/3	0.5/0.9	-0.5±1	2.1±1.7	84/160	-0.005±0.012	0.023±0.0
Sc	75	0.94	7/13	0.8/2	6.2±2.6	11±3.6	49/87	0.13±0.05	0.2±0.07	1/3	0.3/0.6	0.7±1	2.4±1.7	65/110	0.01±0.014	0.034±0.0
Sd	40	0.35	3/5	0.2/0.4	2.8±1.7	4.6±2.2	11/19	0.24±0.15	0.39±0.19	0/0	0/0.1	-0±1	-0.1±1	12/20	-0.004±0.08	-0.008±0.0
Sm	36	0.077	1/5	0.1/0.1	0.9±1	4.9±2.2	2.3/0.7	0.42±0.45	2±0.93	0/1	0/0	-0±1	1±1	2.5/0.8	-0.006±0.41	0.38±
Sbrst	46	0.66	5/13	0.3/0.8	4.7±2.2	12.2±3.6	23/72	0.2±0.09	0.45±0.13	0/3	0.2/0.3	-0.2±1	2.7±1.7	30/92	-0.005±0.03	0.09±0.0
nSbrstL	164	0.75	6/14	1.9/4.4	4.1±2.4	9.6±3.7	89/170	0.05±0.03	0.10±0.04	1/4	0.6/1.3	0.4±1	2.7±2	112/190	0.003±0.009	0.023±0.0
SFRU	88	0.37	1/4	0.7/1.8	0.3±1	2.2±2	22/0.6	0.004±0.036	0.07±0.07	0/0	0.3/0.5	-0.3±1	-0.5±1	31/0.8	-0.009±0.03	-0.017±0.0
SFRA	60	0.57	2/7	0.6/1.3	1.4±1.4	5.7±2.6	30/2.2	0.045±0.05	0.18±0.08	0/3	0.2/0.3	-0.2±1	2.7±1.7	33/2.9	-0.005±0.03	0.08±0.0
SFRB	88	0.79	4/10	1.1/2.9	2.9±2	7.1±3.2	45/23	0.07±0.045	0.13±0.06	0/2	0.5/0.9	-0.5±1	1.1±1.4	65/30	-0.007±0.015	0.016±0.0
SFRC	45	1.4	2/6	0.8/1.7	1.2±1.4	4.3±2.4	48/81	0.025±0.03	0.08±0.05	0/1	0.3/0.5	-0.3±1	0.5±1	56/94	-0.005±0.018	0.008±0.0
SFRD	20	1.7	4/8	0.5/1.2	3.5±2	6.8±2.8	24/140	0.15±0.08	0.24±0.1	1/4	0.2/0.4	0.8±1	3.6±2	33/170	-0.024±0.03	0.11±0.0
SFRE	51	0.56	2/5	0.6/1.1	1.4±1.4	3.9±2.2	25/1.8	0.06±0.06	0.14±0.08	0/2	0.1/0.3	-0.1±1	1.7±1.4	28/2.1	-0.005±0.035	0.06±0.0
SFRF	68	0.69	3/7	0.6/1.9	2.4±1.7	5.1±2.6	26/9.7	0.09±0.07	0.16±0.08	0/1	0.3/0.6	-0.3±1	0.4±1	44/13	-0.008±0.02	0.007±0.0
SFRG	46	1.1	2/7	1/2.1	1±1.4	4.9±2.6	45/38	0.02±0.03	0.10±0.05	0/2	0.3/0.5	-0.3±1	1.5±1.4	50/47	-0.005±0.02	0.03±0.0
SFRH	49	1.5	5/11	0.9/2.2	4.1±2.2	8.8±3.3	53/200	0.08±0.04	0.15±0.06	1/4	0.4/0.7	0.6±1	3.3±2	66/240	0.01±0.015	0.05±0.0

^aThe survey galaxy sample. A 'x' is suffixed when the two peculiar lenticulars NGC1316 and NGC5128 are excluded from the early-type and lenticular sample.

^bNumber of galaxies in this sample.

^cThe average blue light per galaxy in $10^{10} L_{\odot}$.

^dnumber of extra-nuclear X-ray sources observed in this bin, and the cumulative number.

^enumber of predicted background/foreground X-ray sources that would have luminosity in this bin, and the cumulative number

^fthe net number of X-ray sources in this bin, with errors as $\sqrt{N_{ULX}}$.

^gthe cumulative net number of X-ray sources with luminosity of this bin and larger.

^hsurveyed blue light in unit of $10^{10} L_{\odot}$ and the total star formation rate in M_{\odot}/yr for the luminosity in this bin.

ⁱthe ULX rate in unit of ULX per $10^{10} L_{\odot}$ in this bin.

^jthe ULX rate (ULX per $10^{10} L_{\odot}$) for luminosities in this bin and larger.

Table 4. Power-law fits to luminosity functions

galaxies	$lgL_1-lgL_2^a$	α	β	χ_ν^{2b}	Q_ν^c
all	38.4–40	0.56 +0.19 -0.19	1.96 +0.40 -0.29	0.85	0.53
early	38.4–40	0.07 +0.08 -0.07	4.81 +0.63 -2.46	1.20	0.3
late	38.4–40	0.62 +0.21 -0.21	1.73 +0.36 -0.25	0.76	0.6
Sbrst ^d	38.6–40	1.08 +0.47 -0.47	1.73 +0.68 -0.35	0.70	0.62
nSbrstL ^e	39–40	0.55 +0.24 -0.24	1.98 +0.49 -0.27	0.63	0.59

^aThe luminosity interval in which the fit is carried out.

^bThe reduced χ^2 . For a good fit, this is a number not much larger or smaller than one.

^cThe goodness of fit. The model is usually not acceptable if $Q_\nu \ll 1$.

^dThe fit is for the luminosity function in the average survey of starburst galaxies, while for all the first three groups of galaxies the luminosity functions in the deep surveys are used.

^eThe fit is for the luminosity function in the average survey of non-starburst late-type galaxies.

Table 5. Grouping galaxies based on different properties

Group	No. of gal.	lower limit	upper limit	average
group galaxies based on the Hubble type T				
early	91	-6	-1	
late	205	0	11	
peculiar	5	90	99	
elliptical	38	-6	-4	-5
lenticular	53	-3	-1	-2
Sa	45	0	2	1
Sb	77	2	4	3
Sc	75	4	6	5
Sd	40	6	8	7
Sm	36	9	11	10
group galaxies based on star formation rates (M_{\odot}/yr)				
SFRU ^a	102	< 0.009
SFRA	60	...	0.1	0.05
SFRB	88	0.1	1	0.4
SFRC	46	1	4	2.1
SFRD	21	4	...	8.3
SFRE	51	...	0.09	0.04
SFRF	68	0.09	0.5	0.2
SFRG	47	0.5	1.8	1.1
SFRH	50	1.8	...	4.9

^aThis group includes galaxies with only upper limits in the flux densities at 60μ .